Journal of
Water & Climate Change

Check for updates

IWA PUBLISHING

© 2026 The Authors

Journal of Water and Climate Change Vol 17 No 9, 2513 doi: 10.2166/wcc.2026.026

On the determination of pixel-based groundwater withdrawals using SWEO water accounting procedures. Part 2: validation

Tim Hessels [a,*], Wim Bastiaanssen [a,b], Tibor Stigter [c], Jeffrey Davids [d,e], Gerrit Schoups [a] and Chris Perry [f]

[a] Department of Water Management, Faculty of Civil Engineering and Geosciences, Delft University of Technology, Delft, The Netherlands
[b] Hydrosat, Wageningen, The Netherlands
[c] Department of Water Resources and Ecosystems, IHE Delft Institute for Water Education, Delft, The Netherlands
[d] California State University, Chico, CA, USA
[e] Davids Engineering, Chico, CA, USA
[f] Independent Consultant, London, UK
*Corresponding author. E-mail: tmhessels@tudelft.nl; timhessels@hotmail.com

TH, 0000-0002-7264-7220; WB, 0000-0002-7931-5018; TS, 0000-0003-4096-2055; JD, 0000-0003-4343-5410; GS, 0000-0002-2552-7293; CP, 0000-0002-9003-7477

ABSTRACT

The Scalable Water balance from Earth Observation (SWEO) framework proposes an approach to deriving key hydrological fluxes and state variables from remotely sensed data, as a basis for policy formulation and definition of sustainable water allocations. These issues are particularly important in those areas where water is scarce, and current usage depends on unsustainable groundwater use. Validation was carried out across three contrasting basins: the Aconcagua (Chile), Upper North Platte, and Upper San Joaquin (USA) over the period 2003–2019, using the full available dataset. Validation followed four steps combining in situ and independent remote sensing data. First, SWEO monthly total water storage compared well with gravity recovery and climate experiment ($R^2 = 0.62$–0.73). Second, the different water storage components were validated: snow and surface water agreed with United States Department of Agriculture and United States Geological Survey (USGS) observations ($R^2 = 0.84$ and 0.81; MAE = 35.3 mm month^{-1} and 9.59 Mm^3 month^{-1}), and groundwater levels over 17 years matched SWEO ($R^2 = 0.90$; MAE = 10.75 m). Third, SWEO river discharge showed robust agreement with observed streamflow ($R^2 = 0.73$; MAE = 12.48 Mm^3 month^{-1}). Fourth, USGS five-year groundwater reports validated total withdrawals per county, agreeing strongly at basin scale ($R^2 = 0.91$; MAE = 13.79 Mm^3 year^{-1}) and over irrigated areas ($R^2 = 0.90$; MAE = 36.15 mm year^{-1}), with pixel-level patterns matching well density and literature ratios. Overall, SWEO effectively captures monthly water balance dynamics at 250 m resolution across diverse basins, providing a robust tool for long-term water management, allocation policy, and climate impact assessments.

Key words: groundwater recharge, groundwater withdrawals, hydrology, scalable water balance, Scalable Water balance from Earth Observation (SWEO), water accounting

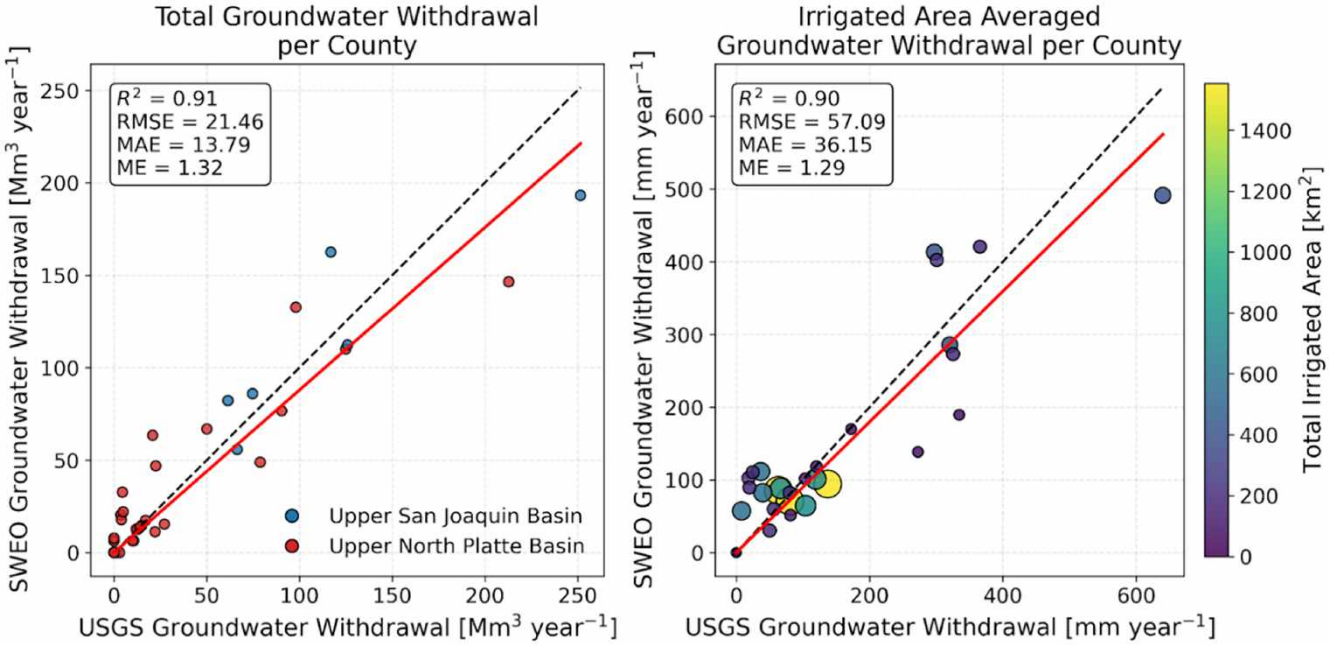
HIGHLIGHTS

- Scalable Water balance from Earth Observation (SWEO): a novel transparent, scalable, remote sensing-based framework for water accounting.
- Closes the water balance at pixel and basin scales.
- Estimates groundwater recharge and withdrawals without detailed hydrogeology.
- Enables groundwater assessment in large and data-scarce regions.

This is an Open Access article distributed under the terms of the Creative Commons Attribution Licence (CC BY 4.0), which permits copying, adaptation and redistribution, provided the original work is properly cited (http://creativecommons.org/licenses/by/4.0/).

Downloaded from iwaponline.com/jwcc/article-pdf/17/9/2513/1637356/jwc2026026.pdf
by Delft University of Technology user

GRAPHICAL ABSTRACT



1. INTRODUCTION

Regions experiencing increasing water stress due to climate variability, agricultural intensification, and population growth are often already dependent on unsustainable groundwater use (Amanambu *et al.* 2020; Rusli *et al.* 2024). Policymakers and planners need objective, reliable, and spatially distributed estimates of groundwater fluxes to formulate and justify appropriate interventions and allocations among water users. While global summaries of hydrological datasets and water management indicators have been developed (Van Ham *et al.* 2018; Yang *et al.* 2021), data sources are often inconsistent or not fully verifiable.

Groundwater systems are complex to describe. They are influenced by interactions with surface water, land use, and climatic drivers, and often lack the observational data (e.g., water levels and withdrawals) required for direct assessment (Sophocleous 2002; Vereecken *et al.* 2016). In consequence, accurate estimation of spatially distributed groundwater fluxes at the basin scale remains particularly challenging.

The scalable water balance from Earth observations (SWEO) framework was developed to provide a robust, transparent, and globally applicable approach for quantifying water availability and use at a monthly time interval (Hessels *et al.* 2022). SWEO leverages satellite-derived precipitation (P) and actual evapotranspiration (ET) to compute rainfall surpluses and deficits (P-ET), capturing not only natural but also anthropogenic water fluxes, including irrigation withdrawals, without requiring explicit reporting of groundwater or irrigation practices. By integrating P-ET with remote sensing measurements of total storage change (ΔS) and, where available, river discharge, SWEO closes the water balance at both basin scale, drainage areas, and the modeling grid ('pixels'). This approach produces physically pixel-based consistent estimates of groundwater recharge, withdrawals, baseflow, percolation, storage change, and lateral flow, without requiring detailed numerical groundwater modeling. Compared with most existing hydrological models and groundwater databases, SWEO provides a transparent, reproducible, and scalable approach that integrates remote sensing datasets to estimate both natural and human-driven groundwater activities. The full methodology is described in detail in the study of Hessels *et al.* (2026). As a newly developed framework, however, the performance and robustness of SWEO across basins with contrasting hydroclimatic and water management conditions still requires systematic validation. Demonstrating that SWEO can reliably reproduce key hydrological fluxes and storage dynamics across contrasting basins is essential before the framework can be confidently applied for water accounting and policy formulation.

Downloaded from iwaponline.com/jwcc/article-pdf/17/9/2513/1637356/jwc2026026.pdf
by Delft University of Technology user

Validation should assess both (1) consistency of the overall water balance and (2) comparison of SWEO-derived groundwater withdrawals with independent measurements. In this paper, SWEO model outputs are validated for three basins that differ in terms of hydroclimate, land use, and water management practices. Using Aconcagua, Upper Platte, and San Joaquin basins, the SWEO water balance estimates are compared with in situ observations and satellite-based data products that were not used to formulate the input data. The results of the validation will provide insights into the accuracy of SWEO, with an emphasis on the spatially distributed groundwater balance data without involving numerical geo-hydrological models.

2. STUDY AREAS

Three river basins were selected for this study to evaluate the SWEO approach under contrasting hydrological and water management conditions over the period 2003–2019, using the full available dataset for model evaluation. These basins were chosen not only because relatively extensive discharge measurements are available and because groundwater abstractions are either documented or the locations of potential withdrawals are known, but also because they represent a range of climatic, hydrological, and irrigation regimes that challenge water accounting methods. The North Platte River Basin primarily relies on surface water for irrigation, whereas the San Joaquin River Basin is heavily dependent on groundwater withdrawals supplemented by surface water. Both basins are highly regulated through extensive reservoir systems and water management infrastructure. In contrast, water availability in the Aconcagua River Basin largely depends on natural snow accumulation and snowmelt in the Andes. However, climate change is shifting the timing of snowmelt, resulting in earlier peak runoff and reduced water availability later in the irrigation season. This diversity ensures that the SWEO framework is tested across basins with varying hydrology, human impacts, and water management practices. The main characteristics of each basin are described in the following sections.

2.1. Study area 1: Aconcagua River Basin, Valparaíso Region, Chile

The Aconcagua River Basin in the Valparaíso Region (Chile) spans an area of approximately 7,340 km^2 and is characterized by a semiarid to Mediterranean climate, see Figure 1. A comprehensive description of the Aconcagua River Basin can be found in the study of Aliaga-Alvarado *et al.* (2023). The study area of this research includes the entire Aconcagua River Basin, extending from its headwaters in the mountains to its outflow point at the Pacific Ocean. This basin was selected because of retiring glaciers, reducing snowmelt, and increasing groundwater abstractions due to expanding irrigation activities (Bastiaanssen & Hessels 2022; Rivera-Vidal *et al.* 2025). In the Aconcagua basin, these dynamics have led to a condition of groundwater overdraft (Alvarez-Garreton *et al.* 2024). This case exemplifies a typical situation in semiarid regions, where unsustainable groundwater use necessitates the development of comprehensive water management strategies to enhance climate resilience.

2.2. Study area 2: Upper San Joaquin River Basin, California, United States of America

The San Joaquin River Basin is situated in the Sierra Nevada region of central California and covers a predominantly mountainous, high-elevation area in its upstream reaches. Extensive agricultural plains are present in the downstream area. In this study, the upper part of the San Joaquin Basin is taken into account (5,266 km^2), see Figure 2. The downstream boundary of the basin is defined at the outflow point of the San Joaquin River near Mendota. The San Joaquin River Basin contains an extensive network of irrigation canals. Focusing solely on the upper area of the San Joaquin River Basin is necessary because the hydrological system is strongly influenced by human regulation. Reliable observations are required to accurately represent the anthropogenic effects of aqueducts importing snowmelt water from the Sierra Nevada and groundwater withdrawals for almonds, pistachios, and grape orchards. The section of the basin selected for this study corresponds to an area where both inflows and outflows of these artificial canals are well monitored throughout the modeling period.

2.3. Study area 3: North Platte River Basin, Nebraska, United States of America

The North Platte River Basin spans parts of Colorado, Wyoming, and Nebraska. The basin includes a varied landscape characterized by the mountainous landscape of the Rocky Mountains and transitioning downstream into arid high plains and extensive agricultural lands. In this study, the upper portion of the North Platte River Basin is excluded from the model domain, as it consists primarily of natural areas with minimal human irrigation influence. The surface water inflow from the upstream area is introduced at the basin entry point and used as a boundary condition. The downstream boundary of the basin is defined at the outflow point of the North Platte River near Scottsbluff, which drains an area of

Downloaded from iwaponline.com/jwcc/article-pdf/17/9/2513/1637356/jwc2026026.pdf
by Delft University of Technology user

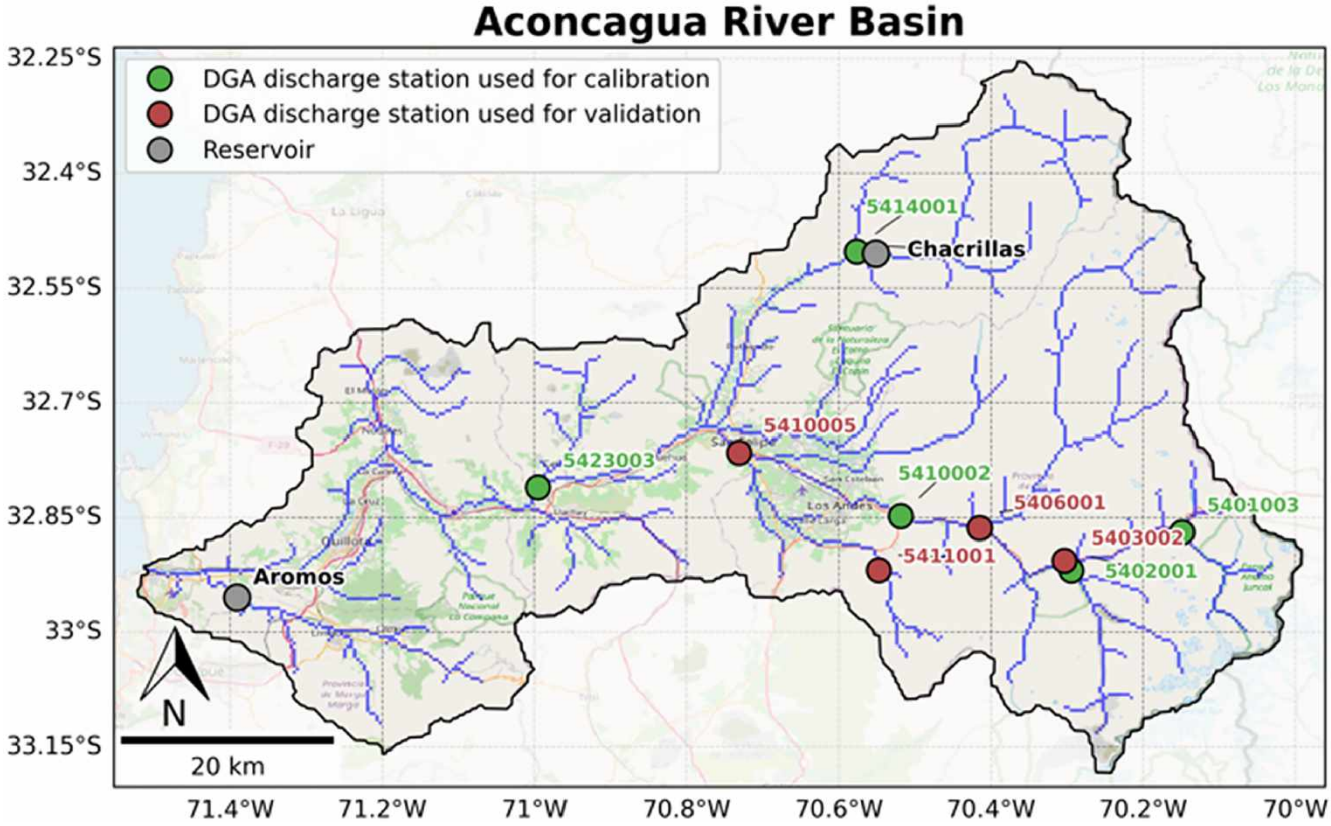


Figure 1 | Overview of the Aconcagua River Basin as represented in this study, including the locations of discharge stations. Five discharge stations are used for model calibration and four discharge stations for model validation.

57,331 km^2, see Figure 3. The North Platte Natural Resources District is focusing on (i) understanding water use and how it has changed over time, (ii) better understanding of both surface and groundwater to determine if the Integrated Management Plan goals are being met, (iii) how drought, conservation measures, and groundwater pumping affect the whole water system, and (iv) providing an evaluation of management decisions. A great set of tools is being used for this purpose, and it is interesting to compare existing advanced modeling tools with SWEO, which has an open-access character essentially.

3. MATERIALS

The SWEO framework as described in detail by Hessels *et al.* (2026) which was tested for the three river basins. Topography and drainage direction data were obtained from HydroSHEDS version 1.0 (Warmedinger *et al.* 2023). Land cover classification was based on the National Land Cover Database product for basins in the USA (USGS 2020) and the MapBiomas Chile Collection 1.0 for the Chilean basin (MapBiomas 2024). Soil physical and hydraulic properties were extracted from the SoilGrids v2.0.1 dataset (Hengl *et al.* 2017). The spatial variation of initial groundwater table depth on 1 January 2003 was taken from the global hydrological PCRaster Global Water Balance (PCR-GLOBWB) model (Wada *et al.* 2014; Sutanudjaja *et al.* 2018). Monthly surface water extent was derived from the Joint Research Centre (JRC) Global Surface Water dataset, version 1.4 (Pekel *et al.* 2016). Monthly reference evapotranspiration data were derived from the Famine Early Warning Systems Network (FEWS NET) Land Data Assimilation System, version 6.0 (FEWS V6.0). Monthly atmospheric temperatures were obtained from the MERRA-2 reanalysis dataset (MERRA V2). Vegetation characteristics, such as the fraction of photosynthetical active radiation and leaf area index, were incorporated through the 8-day moderate resolution imaging spectroradiometer (MODIS), specifically MOD15A2H.061, which were aggregated to monthly temporal resolution. Snow cover data were sourced from the 8-day MODIS MOD10A3.061 product and similarly aggregated to monthly values.

Daily precipitation estimates were taken from the Climate Hazards Group InfraRed Precipitation with Station data (CHIRPS) version 2.0 dataset (Funk *et al.* 2015). The *P*-values were validated and bias corrected using local gauge

Downloaded from iwaponline.com/jwcc/article-pdf/17/9/2513/1637356/jwc2026026.pdf
by Delft University of Technology user

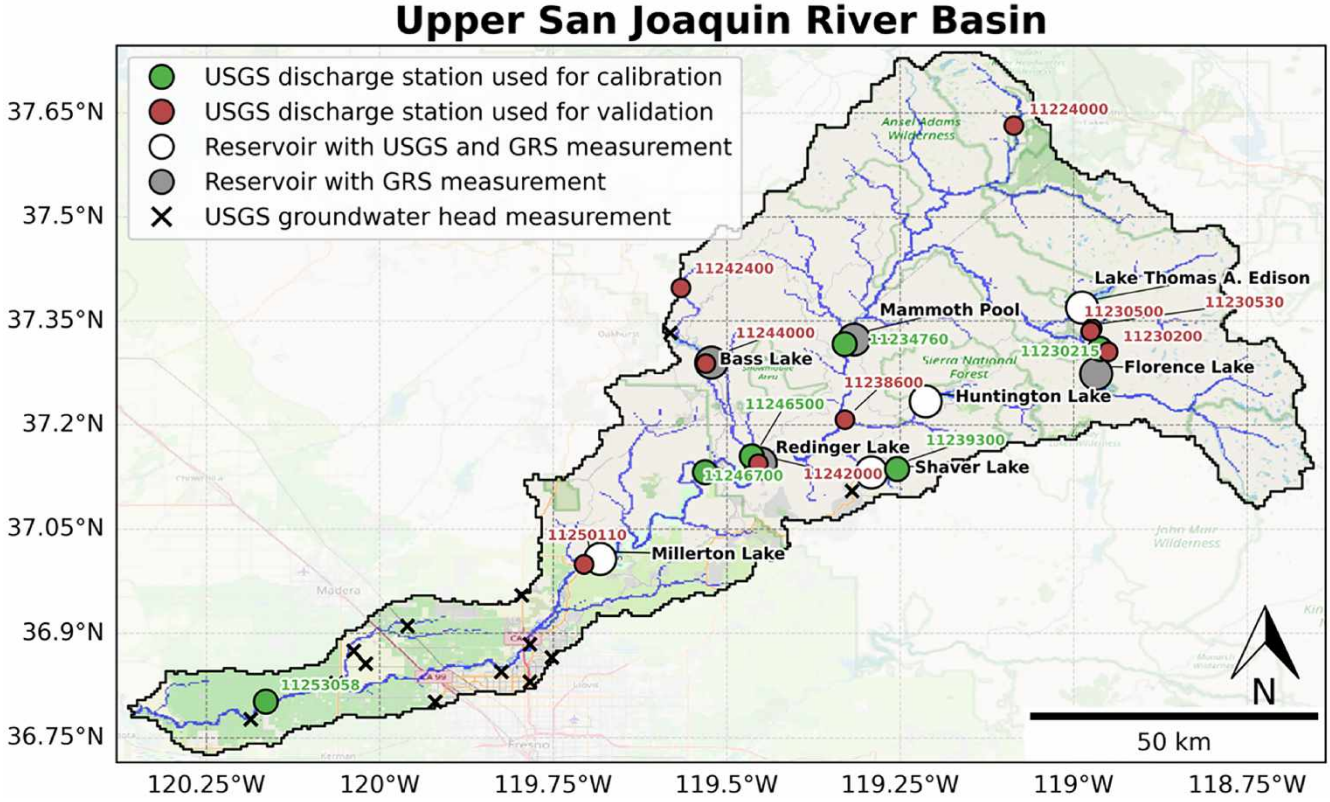


Figure 2 | Overview of the Upper San Joaquin River Basin as represented in this study, including the locations of discharge stations. Six discharge stations are used for model calibration and nine for model validation.

measurements, following approaches commonly reported in the literature (e.g., Dinku *et al.* 2014; Hessels 2015; López-Bermeo *et al.* 2022).

For monthly actual evapotranspiration, the ensemble product from OpenET version 2.0 was used for the basins located in the USA (Melton *et al.* 2025), while evapotranspiration for the Chilean basin was derived using the ETLook-based algorithm (Bastiaanssen *et al.* 2012) that forms the basis for the Food and Agriculture Organization (FAO) WaPOR version 2.0 algorithm (FAO 2020). Basin-wide ET values were utilized to derive a single bias correction factor for ET, which was subsequently applied to all pixels. The determination and application of this bias correction were carried out within the SWEO framework and were based on the consistency of the long-term basin-wide water balance (step 1 in the model, see Hessels *et al.* 2026). A similar approach for developing bias corrections in Thailand watersheds was done by Sriwongsitanon *et al.* (2020). Many papers deal with the validation of ET from remote sensing (e.g., Karimi & Bastiaanssen 2015; Ren *et al.* 2025). SWEO internally calibrates ET using terrestrial water storage anomalies retrieved from the gravity recovery and climate experiment (GRACE) Level-3 mascon product (version RL06M, solution V02.3b) (Wiese *et al.* 2019). This dataset was employed to calibrate ET across a long period (2003–2019) because 17-year total water storage changes are relatively minor.

In addition, discharge measurements have been used for the internal calibration of both total water storage and surface runoff. For this purpose, data from the United States Geological Survey (USGS) and Dirección General de Agua (DGA) were utilized, providing observed streamflow information. The use of both GRACE data and discharge measurements for internal calibration is described in detail in the accompanying methodology paper.

An overview of the input datasets for the SWEO model is presented in Table 1.

Table 2 presents an overview of the datasets used for validating the SWEO model, detailing the type of data, spatial and temporal coverage, and sources. These datasets include a combination of remotely sensed products, in situ measurements, and administrative records, covering key hydrological variables such as terrestrial water storage, snow water equivalent, surface water storage, groundwater levels, discharge measurements, groundwater withdrawals, and locations of groundwater extraction rights. Together, they provide independent benchmarks for assessing the performance of the SWEO model.

Downloaded from iwaponline.com/jwcc/article-pdf/17/9/2513/1637356/jwc2026026.pdf
by Delft University of Technology user

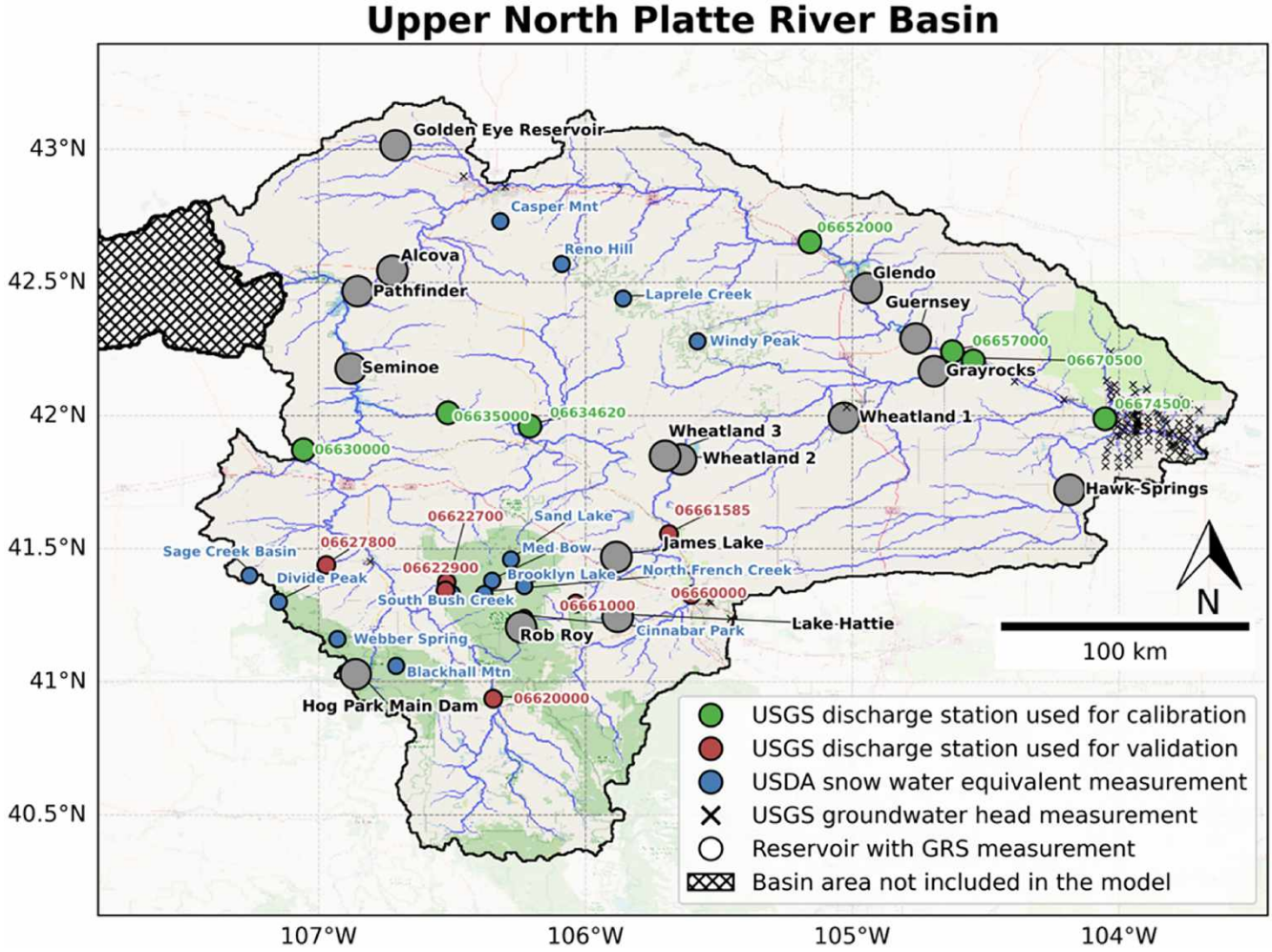


Figure 3 | Overview of the North Platte River Basin as represented in this study, including the locations of discharge stations. Seven discharge stations are used for model calibration and seven for model validation.

4. METHODS

The validation is conducted in four consecutive steps. First, the consistency of the overall water balance is evaluated (steps i–iii), after which groundwater withdrawals are assessed (step iv).

As a first step, the monthly change in total water storage (ΔS_{tot}) is evaluated. Due to the basin's capacity to store water, fluxes at the land surface do not directly translate into river discharge. ΔS_{tot}, therefore, plays a key role in buffering water during wet periods and releasing it during dry periods. ΔS_{tot} at the (sub)basin level is calculated as the difference between total monthly inflows and outflows:

$$\Delta S_{tot} = P + R_{in} + C_{in} - R_{out} - I - ET - Q_{lat} \quad (1)$$

where P is the precipitation (mm month^{-1}), ET is the evapotranspiration (mm month^{-1}), I is the interception (mm month^{-1}), ΔS_{tot} is the total change in water storage (mm month^{-1}), R_{in} is the total river inflow (mm month^{-1}), R_{out} is the total river outflow (mm month^{-1}), C_{in} is the net canal discharge, representing water transferred between basins through aqueducts (mm month^{-1}), and Q_{lat} is the net lateral groundwater outflow, exiting through groundwater layers (mm month^{-1}).

In water accounting, it is essential to independently verify estimates of monthly ΔS_{tot}, rather than relying solely on the water balance, to ensure consistency with observed conditions. GRACE measures temporal variations in Earth's gravity

Downloaded from iwaponline.com/jwcc/article-pdf/17/9/2513/1637356/jwc2026026.pdf
by Delft University of Technology user

Downloaded from iwaponline.com/jwcc/article-pdf/17/9/2513/1637356/jwc2026026.pdf
by Delft University of Technology user

Table 1 | Overview of SWEO input data used in this study

Parameter	Product	Version	Temporal resolution	Spatial resolution	Source	Provider/URL
Precipitation	CHIRPS	v2.0	daily	0.05°	Climate Hazards Center (UCSB)	https://data.chc.ucsb.edu/products/CHIRPS-2.0
Evapotranspiration (Chile)	pyWAPOR	v2.0	8-daily	250–300 m	FAO	https://bitbucket.org/cioapps/pywapor/src/master
Evapotranspiration (USA)	OpenET	Ensemble V2.0	monthly	30 m	Open ET, Inc.	Google Earth Engine
Reference evapotranspiration	FEWS	v6.0	daily	0.1°	USGS/FEWS NET	https://edcintl.cr.usgs.gov/downloads/sciweb1/shared/fews/web/global/daily/pet/downloads/daily
Air temperature	MERRA	v2	monthly	0.5° × 0.625°	NASA GMAO	https://goldsmr4.gesdisc.eosdis.nasa.gov/data/MERRA2/M2I1NXASM.5.12.4
Leaf area index	MOD15	Collection 6.1	8-daily	400–500 m	NASA LP DAAC	https://e4ftl01.cr.usgs.gov/MOLT/MOD15A2H.061
Photosynthetical active radiation	MOD15	Collection 6.1	8-daily	400–500 m	USGS LP DAAC	https://e4ftl01.cr.usgs.gov/MOLT/MOD15A2H.061
Snow cover	MOD10	Collection 6.1	8-daily	400–500 m	USGS LP NSIDC	https://n5eil01u.ecs.nsidc.org/MOST/MOD10A2.061
Groundwater storage	GRACE	version RL06M, solution V02.3b	+/– Monthly	~300 km	NASA JPL	https://podaac.jpl.nasa.gov/dataset/TELLUS_GRAC-GRFO_MASCON_CRI_GRID_RL06_V2
Water body area	JRC Global Surface Water	v1.4	Monthly	30 m	European Commission JRC	Google Earth Engine Catalog
Altitude and drainage direction	HydroSHED	v1	–	3 arc-sec	WWF/ USGS	https://www.hydrosheds.org/hydrosheds-core-downloads
Land cover (Chile)	MapBiomas Chile	Collection 1.0	–	30 m	MapBiomas	https://chile.mapbiomas.org/en/mapas-de-la-coleccion
Land cover (USA)	NLCD	Collection 1.0	–	30 m	USGS MRLC	https://www.mrlc.gov/data
Soil properties	Soilgrids	v2.0.1	–	250 m	ISRIC	https://maps.isric.org
Piezometric heads and fluctuations	PCR-GLOBWB	v2	Monthly	5 arc-min	Utrecht University	https://globalhydrology.nl/research/models/pcr-globwb-2-0
Discharge measurement (Chile)	–	–	Daily	–	DGA	https://snia.mop.gob.cl
Discharge measurement (USA)	–	–	Daily	–	USGS	http://nwis.waterdata.usgs.gov

Table 2 | Overview of the validation datasets used to evaluate the SWEO model, including data type, spatial and temporal coverage, and source

Parameter	Product	Version	Temporal resolution	Spatial resolution	Source	Provider/URL
Total water storage	GRACE	version RL06M, solution V02.3b	+/- Monthly	~300 km	NASA JPL	https://podaac.jpl.nasa.gov/dataset/TELLUS_GRAC-GRFO_MASCON_CRI_GRID_RL06_V2
Snow water equivalent (USA)	SNOTEL	–	Daily	–	USDA	https://wcc.sc.egov.usda.gov/reportGenerator
Surface water storage (USA)	–	–	Daily	–	USGS	http://nwis.waterdata.usgs.gov
Surface water storage	Global reservoir storage (GRS)	V1	Monthly	–	Li (2023)	https://zenodo.org/records/7855477
Groundwater level (USA)	–	–	–	–	USGS	http://nwis.waterdata.usgs.gov
Discharge measurement (Chile)	–	–	Daily	–	Dirección General de Aguas, DGA	https://snia.mop.gob.cl
Discharge measurement (USA)	–	–	Daily	–	USGS	http://nwis.waterdata.usgs.gov
Groundwater withdrawal (USA)	USGS Water Use Reports	2005, 2010, 2015	5-yearly	county	USGS	https://pubs.usgs.gov/circ/1344 https://pubs.usgs.gov/circ/1405 https://pubs.usgs.gov/publication/cir1441
Groundwater extraction rights (Chile)	–	2025-04-16	–	–	DGA	https://dga.mop.gob.cl/derechos-de-agua/derechos-registrados/
Groundwater well permits (USA)	WSEO	2010–2011	–	–	WSEO/WSGS	https://waterplan.state.wy.us/plan/platte/2013/gis/Wells_WSEO_PtRB.html

field, which can be used to infer changes in terrestrial water storage, including groundwater, snow, soil moisture, and surface water (Tapley *et al.* 2004). Although the SWEO framework primarily calibrates ET based on the long-term ΔS_{tot} trend using the first and last GRACE observations of the modeling period, the monthly GRACE mascon time series remains valuable for independent validation of ΔS_{tot} on a monthly time scale. The key question, therefore, is whether the monthly ΔS_{tot} estimated by SWEO from the overall water balance [Equation (1)] is consistent with the monthly ΔS_{tot} by GRACE.

The second step focuses on the individual storage components. Within the SWEO framework, changes in groundwater storage (ΔS_{gw}) are estimated at the pixel level as the residual component of ΔS_{tot} after accounting for changes in snow storage (ΔS_{snow}), surface water storage (ΔS_{sw}), and subsurface soil moisture storage (ΔS_{θ}). This residual approach is used because these other storage components can generally be estimated more directly than ΔS_{gw}. To ensure that the resulting estimate of ΔS_{gw} is reliable, the contributing storage components (ΔS_{snow}, ΔS_{sw}, and ΔS_{θ}) are first evaluated using independent observations. Additionally, groundwater heads derived from ΔS_{gw} are compared with observed groundwater head measurements to further validate the estimates.

The third step provides a final consistency check of the overall water balance, based on pixel-scale water surpluses that also include the storage change components (ΔS_{sw}, ΔS_{snow}, ΔS_{θ}, and ΔS_{gw}). Consistency between these fluxes and storage states is crucial, as errors in any term can propagate and lead to unrealistic discharge dynamics. Therefore, the monthly changes in the four storage components within a drainage area can be validated using observed monthly river flow.

Downloaded from iwaponline.com/jwcc/article-pdf/17/9/2513/1637356/jwc2026026.pdf
by Delft University of Technology user

The expected pixel-based flow Q in SWEO is obtained by calculating the upstream surplus (Q_{pix}) of all pixels:

$$Q_{\text{pix}} = P - ET - I - Q_{\text{lat}} - \Delta S_{sw} - \Delta S_{\text{snow}} - \Delta S_{\theta} - \Delta S_{gw} + R_{\text{in}} + C_{\text{in}} - R_{\text{out}} \quad (2)$$

Using a drainage direction map derived from surface elevation data, Q_{pix} values are routed and summed to obtain discharge for each pixel. The simulated discharge is compared with measured river discharge at gauging stations that were not used for model calibration.

Lastly, after these consistency checks of the overall water balance, groundwater withdrawal volumes and their spatial distribution are validated against reported groundwater withdrawals. For the basins located in the USA, the groundwater withdrawal estimates derived from SWEO are validated against reported groundwater withdrawal data from the USGS. Five-yearly USGS groundwater-use reports for the years 2005 (Kenny *et al.* 2009), 2010 (Maupin *et al.* 2014), and 2015 (Dieter *et al.* 2018) were used, which provide county-level totals of groundwater withdrawals for agricultural purposes. These reported values are compared with modeled groundwater withdrawals from SWEO at the county scale on a yearly basis. The USGS reports have not been used for the formulation of the input data. For counties that were only partially covered by the modeled basin, reported groundwater withdrawals were rescaled using the ratio of irrigated agricultural area within the study area to the total irrigated area of the county. Following this procedure, groundwater withdrawal estimates were compared for a total of 13 counties for the years 2005, 2010, and 2015.

Validation at the individual field level is more challenging, as a single pump installation may supply groundwater to multiple agricultural fields. Instead, the fraction of groundwater withdrawals (Q_{gw}) over total water withdrawals (Q_{tot}) fractions were verified. Because well abstraction density serves as a useful proxy for the relative contribution of groundwater to irrigation supply, areas with a higher density of wells are expected to exhibit a larger fraction of groundwater withdrawals relative to surface water. Consequently, the locations of these groundwater abstraction points in the Aconcagua Basin and the Upper North Platte River Basin provide an independent data source for assessing $Q_{\text{gw}}/Q_{\text{tot}}$ fractions from SWEO.

In summary, the validation consists of the following four steps:

(i) Monthly values of ΔS_{tot} derived from the water balance and discharge measurements are validated against GRACE-based estimates.
(ii) The decomposed components of ΔS_{tot} (ΔS_{gw}, ΔS_{snow}, ΔS_{sw}, and ΔS_{θ}) are evaluated using independent observations.
(iii) Internal consistency of the water balance is assessed by verifying whether storage changes and fluxes reproduce measured river outflow from a subbasin on a monthly basis.
(iv) Finally, estimated groundwater withdrawals are validated by comparing total withdrawal volumes with reported withdrawals in major irrigated areas and by evaluating their spatial distribution against the density of well permits.

Model performance is evaluated using the coefficient of determination (R^2), root mean square error (RMSE), mean absolute error (MAE), and mean error (ME). These are determined by:

$$R^2 = 1 - \frac{\sum_{i=1}^{n} (y_i - \hat{y}_i)^2}{\sum_{i=1}^{n} (y_i - \bar{y})^2} \quad (3)$$

$$\text{RMSE} = \sqrt{\frac{1}{n} \sum_{i=1}^{n} (\hat{y}_i - y_i)^2} \quad (4)$$

$$\text{MAE} = \frac{1}{n} \sum_{i=1}^{n} |\hat{y}_i - y_i| \quad (5)$$

$$\text{ME} = \frac{1}{n} \sum_{i=1}^{n} (\hat{y}_i - y_i) \quad (6)$$

where y_i is the observed value, $\hat{y}_i$ is the predicted value, $\bar{y}_i$ is the mean of observed values, and n is the number of observations.

Downloaded from iwaponline.com/jwcc/article-pdf/17/9/2513/1637356/jwc2026026.pdf
by Delft University of Technology user

In the context of water accounting, .particular emphasis is placed on R^2 and MAE. R^2 quantifies how well the temporal variability and seasonal dynamics are reproduced, while MAE measures the average magnitude of deviations between modeled and observed values in the same units as the water balance components.

ME and RMSE are additionally evaluated to provide insight into the error structure. ME indicates systematic bias, with values close to zero suggesting that over- and underestimations balance out, while positive or negative values indicate consistent over- or underestimation. RMSE, which squares the errors, is more sensitive to large deviations and highlights the influence of occasional outliers. When RMSE is substantially larger than MAE, it indicates that the overall error is dominated by a few large discrepancies rather than by systematic deviations across the time series.

5. RESULTS AND DISCUSSION

5.1. Step (i): validation of total water storage

Across all three study basins, SWEO-based ΔS_{tot} successfully reproduces both the seasonal cycle and interannual variability of total water storage (TWS) changes observed by GRACE. Figure 4 shows the time series for the Upper North Platte River Basin where January 2003 is taken as a zero value. Hence, the graph depicts the storage changes across a period of 17 years. The characteristic pattern of increasing storage during winter and depletion during summer is consistently captured, as are wetter and drier years. Figure 5 presents the basin-scale scatterplots of monthly ΔS_{tot} values from SWEO versus GRACE. The R^2 between 250 m SWEO values of ΔS_{tot} and 300 km GRACE-derived ΔS_{tot} values ranges between 0.62 and 0.73, indicating good agreement given the scale mismatch between the two datasets.

The accuracy of the GRACE product decreases toward the end of the lifetime of the first GRACE satellite mission, resulting in reduced data quality (Śliwińska *et al.* 2020a). This degradation is also reflected in the SWEO comparison, where larger discrepancies between SWEO and GRACE are observed for the period 2014–2018. The GRACE data from the first satellite mission are considered most reliable during the period 2006–2014 (Śliwińska *et al.* 2020b; Murböck *et al.* 2023). Consistently, this period also shows the smallest differences between SWEO and GRACE.

Differences in absolute magnitude are expected, particularly in hydrologically heterogeneous basins where localized reservoirs, lakes, or snowpacks are not fully captured by GRACE mascon products. This results in a relatively high MAE of 38.9 mm month^{-1} for the Upper San Joaquin Basin, whereas the larger and less heterogeneous Upper North Platte River Basin exhibits a lower MAE of 7.6 mm month^{-1}. Nevertheless, because the first and last GRACE values are used to calibrate ET, the ME remains nearly zero across all basins.

5.2. Step (ii): validation of individual water storage components

ΔS_{tot} in SWEO is decomposed into four components: ΔS_{snow}, ΔS_{sw}, ΔS_{θ}, and ΔS_{gw}. Each component is explicitly validated to assess its contribution to the accuracy of monthly total water storage.

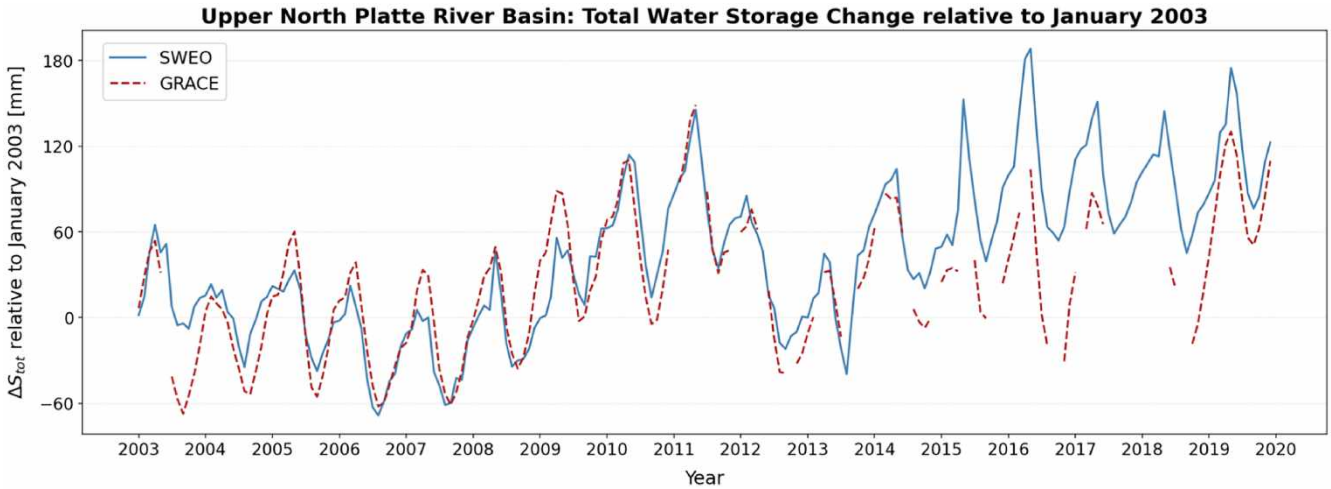


Figure 4 | Comparison of groundwater storage over the entire Upper North Platte Basin derived from SWEO and GRACE, with groundwater storage in January 2003 normalized to 0 mm.

Downloaded from iwaponline.com/jwcc/article-pdf/17/9/2513/1637356/jwc2026026.pdf
by Delft University of Technology user

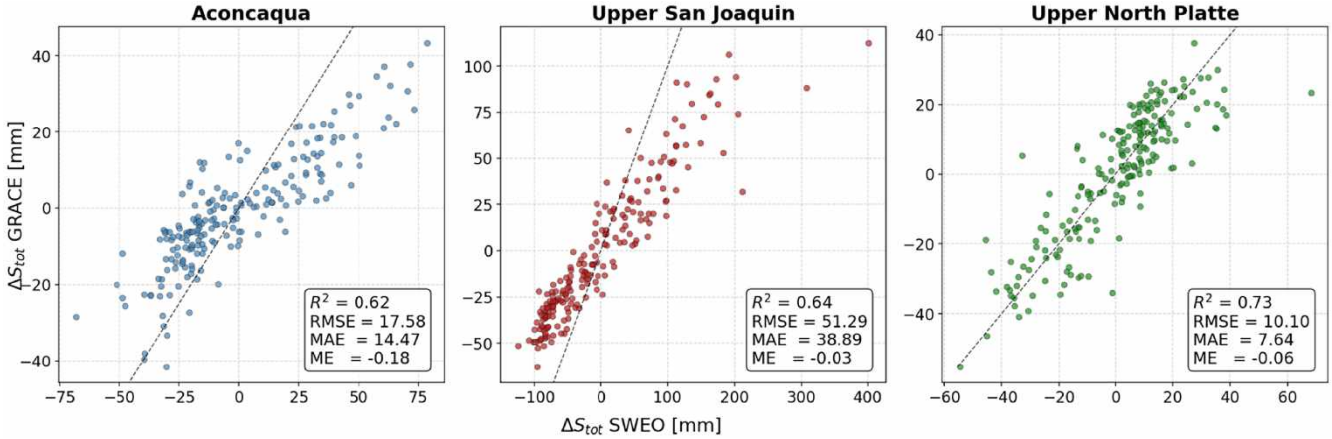


Figure 5 | Correlation analysis between monthly river basin storage changes from SWEO water accounting based on P, ET, I and Q, and GRACE observations. A 1:1 line is also shown for reference.

ΔS_{snow} was validated using measurements from 14 Snow Telemetry (SNOTEL) stations in the North Platte River Basin (USDA 2025). Table 3 presents R^2, RMSE, MAE, and ME for each station. Overall, SWEO-derived ΔS_{snow} shows strong agreement with observed ΔS_{snow}, calculated from SWE differences, with an average R^2 of 0.84 and an average MAE of 35.3 mm month^{-1}, corresponding to 19% of the mean absolute monthly observed ΔS_{snow}. The largest differences occur during the melting season, when SNOTEL measurements indicate faster snowmelt than SWEO at the start of the growing season. Figure 6 illustrates the scatterplot of ΔS_{snow} for Windy Peak.

Cumulative ΔS_{snow} provides total snow storage (S_{snow}). SWEO accurately captures the seasonal accumulation and melt dynamics, including the timing of peak snow storage, as shown in Figure 7 for Windy Peak. Across all SNOTEL stations, SWEO slightly underestimates S_{snow} by approximately 25%, mainly due to a small underestimation of winter snowfall in these mountainous regions. This contributes to a reduced total snowpack and less snowmelt at the onset of the growing season.

Table 3 | Statistical comparison of snow storage change derived from SWEO and SNOTEL observations (USDA 2025) for selected stations in the Upper North Platte River Basin, including the coefficient of determination (R^2), root mean square error (RMSE; mm month^{-1}), mean absolute error (MAE; mm month^{-1}), and mean error (ME; mm month^{-1})

Basin	Station	Coordinates (WGS84)	Source	R^2	RMSE	MAE	ME
North Platte River	Windy Peak	N: 42.28°, E: −105.58°	USDA	0.80	26.86	16.68	−0.15
North Platte River	Laprele Creek	N: 42.44°, E: −105.86°	USDA	0.79	30.40	19.06	−0.35
North Platte River	Reno Hill	N: 42.57°, E: −106.09°	USDA	0.84	42.25	25.57	−0.38
North Platte River	Casper Mountain	N: 42.73°, E: −106.32°	USDA	0.83	41.62	24.49	−0.34
North Platte River	Sand Lake	N: 41.46°, E: −106.28°	USDA	0.85	85.88	54.22	−0.14
North Platte River	Med Bow	N: 41.38°, E: −106.35°	USDA	0.86	94.00	61.78	−2.54
North Platte River	North French Creek	N: 41.33°, E: −106.38°	USDA	0.87	78.11	49.87	−0.03
North Platte River	South Bush Creek	N: 41.33°, E: −106.50°	USDA	0.82	36.86	23.27	−0.10
North Platte River	Brooklyn Lake	N: 41.36°, E: -106.23°	USDA	0.86	62.53	37.01	−0.15
North Platte River	Cinnabar Park	N: 41.24°, E: −106.23°	USDA	0.85	52.72	33.58	−0.49
North Platte River	Blackhall Mountain	N: 41.06°, E: −106.71°	USDA	0.86	86.92	53.77	−0.91
North Platte River	Webber Spring	N: 41.16°, E: −106.93°	USDA	0.86	60.25	38.56	−0.40
North Platte River	Sage Creek Basin	N: 41.40°, E: −107.26°	USDA	0.84	40.19	25.41	−0.31
North Platte River	Divide Peak	N: 41.30°, E: −107.15°	USDA	0.85	52.94	32.24	−0.32
		Total Average		0.84	56.5	35.3	−0.47

Downloaded from iwaponline.com/jwcc/article-pdf/17/9/2513/1637356/jwc2026026.pdf
by Delft University of Technology user

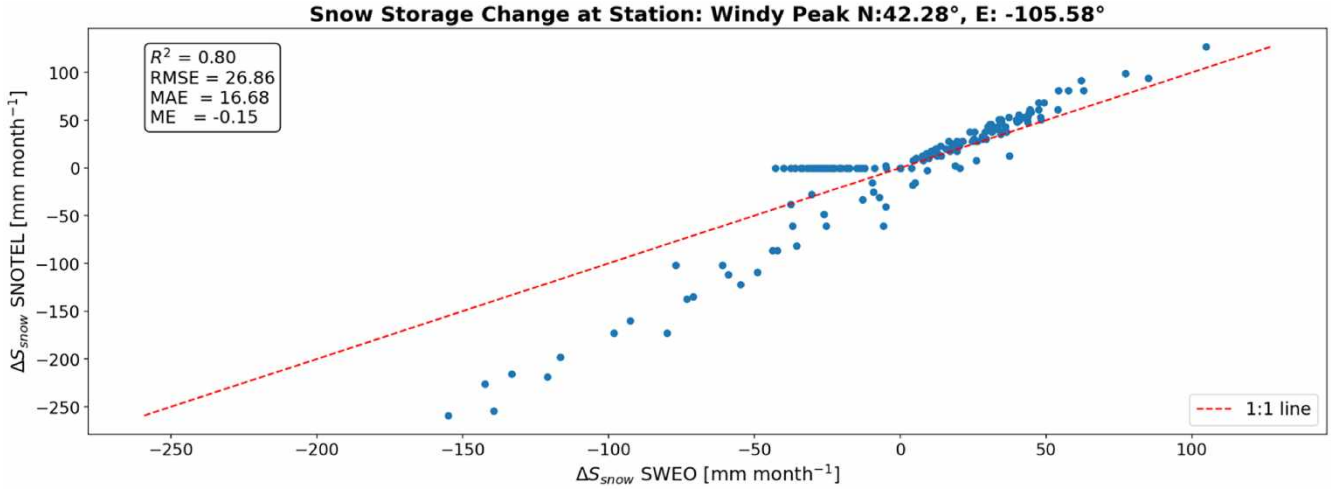


Figure 6 | Correlation analysis between snow storage changes from SWEO and SNOTEL observations (USDA 2025) at the Windy Peak station in the Upper North Platte River Basin.

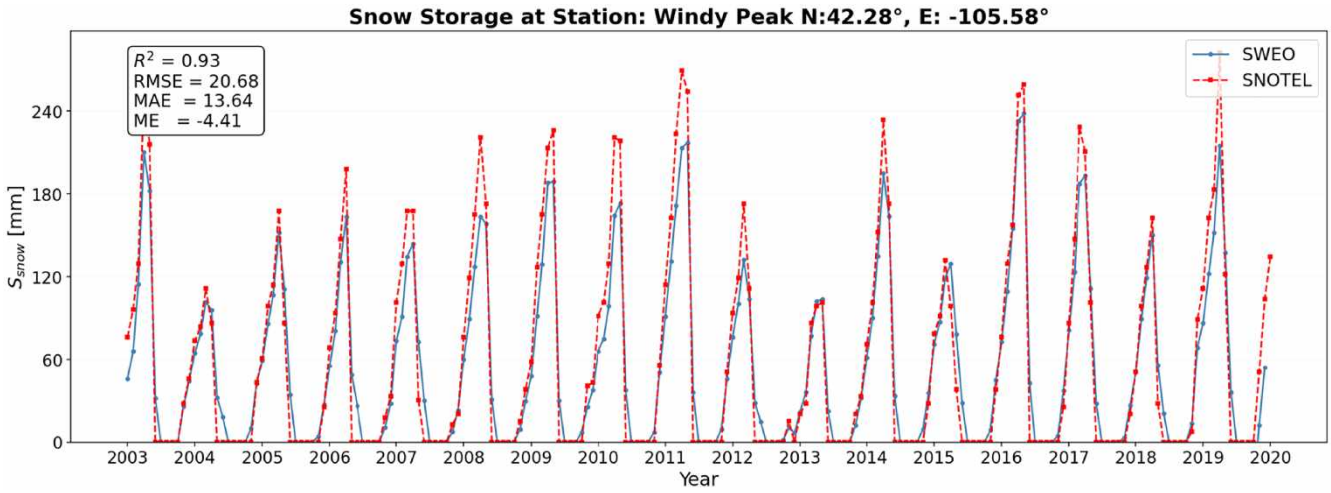


Figure 7 | Comparison between SWEO and SNOTEL total snow storage for Windy Peak station located in the Upper North Platte River Basin.

These results demonstrate that SWEO reliably represents snow-related storage changes, which are critical for seasonal runoff estimation. Minor underestimations during the early melting period reflect a slightly slower snowmelt and lower peak snow storage in SWEO, but overall the model provides a robust representation of snow dynamics.

ΔS_{sw} was validated against observed reservoir volume changes derived from 4 USGS gauging stations (USGS 2025) and 15 estimates based on the global reservoir storage (GRS) dataset that is based on measured inflow and outflow (Li 2023). The results of the comparison are shown in Table 4. Overall, the average R^2 for all reservoirs is 0.60, indicating reasonable agreement. For the 4 reservoirs with USGS observations, SWEO-derived ΔS_{sw} shows much stronger agreement, with an average R^2 of 0.81 and average MAE of 9.6 Mm^3 month^{-1}, corresponding to 22% of the mean absolute monthly observed ΔS_{sw}. In contrast, the agreement between SWEO-derived ΔS_{sw} and the GRS dataset is lower, with an average R^2 of 0.57. To assess the reliability of the GRS database for these regions, the four USGS-monitored reservoirs were compared directly with GRS-derived storage estimates. Although not shown, the results reveal a relatively low R^2 of 0.19. This suggests limited agreement for those reservoirs and justifies placing greater reliance on validation based on USGS data when evaluating SWEO's performance for these regions. Figures 8–11 present the time series and scatterplots of ΔS_{sw} for the relatively small Lake Thomas A. Edison and the large Pathfinder Reservoir, demonstrating strong agreement.

Downloaded from iwaponline.com/jwcc/article-pdf/17/9/2513/1637356/jwc2026026.pdf
by Delft University of Technology user

Table 4 | Statistical comparison of surface water storage changes derived from SWEO with USGS observations or GRS estimates for selected reservoirs in the Upper San Joaquin and Upper North Platte River Basins, including the coefficient of determination (R^2), root mean square error (RMSE; Mm^3 $month^{-1}$), mean absolute error (MAE; Mm^3 $month^{-1}$), and mean error (ME; Mm^3 $month^{-1}$)

Basin	Reservoir	Lake Area (km^2)	Source	R^2	RMSE	MAE	ME
Upper San Joaquin	Bass Lake	3.8	GRS	0.68	1.76	1.23	−0.12
Upper San Joaquin	Florence Lake	1.9	GRS	0.70	8.38	5.82	−0.59
Upper San Joaquin	Huntington Lake	4.8	USGS	0.89	6.59	4.60	−0.03
Upper San Joaquin	Lake Thomas A. Edison	6.7	USGS	0.84	7.46	4.71	0.09
Upper San Joaquin	Mammoth Pool	2.7	GRS	0.63	36.05	10.36	7.86
Upper San Joaquin	Millerton Lake	15.8	USGS	0.91	31.96	22.15	0.37
Upper San Joaquin	Redinger Lake	1.2	GRS	0.66	0.83	0.60	−0.01
Upper San Joaquin	Shaver Lake	7.8	USGS	0.61	12.29	6.90	0.10
Upper North Platte River	Alcova	8.1	GRS	0.31	6.20	2.68	−0.29
Upper North Platte River	Glendo	36.0	GRS	0.75	46.51	36.22	−5.16
Upper North Platte River	Golden Eye Reservoir	1.5	GRS	0.68	0.18	0.11	−0.02
Upper North Platte River	Grayrocks	13.5	GRS	0.66	2.79	1.75	−0.11
Upper North Platte River	Guernsey	6.8	GRS	0.50	6.41	5.05	−0.59
Upper North Platte River	Hawk Spring	3.7	GRS	0.58	1.73	1.28	−0.19
Upper North Platte River	Hog Park Main Dam	2.0	GRS	0.21	1.68	0.74	−0.11
Upper North Platte River	James Lake	2.3	GRS	0.65	0.33	0.17	−0.01
Upper North Platte River	Lake Hattie	7.8	GRS	0.22	0.97	0.57	−0.03
Upper North Platte River	Pathfinder	75.1	GRS	0.72	47.59	29.62	−3.61
Upper North Platte River	Rob Roy	2.7	GRS	0.29	1.28	0.9	−0.03
Upper North Platte River	Seminoe	57.2	GRS	0.71	37.19	22.71	−1.30
Upper North Platte River	Wheatland 1	1.4	GRS	0.73	0.59	0.45	−0.06
Upper North Platte River	Wheatland 2	22.6	GRS	0.52	5.92	4.62	−0.59
Upper North Platte River	Wheatland 3	13.1	GRS	0.61	3.49	1.56	−0.13
		Total average		0.60	11.66	7.16	−0.19
		Average over USGS		0.81	12.29	9.59	0.13
		Average over GRS		0.57	11.04	6.65	

ΔS_θ constitutes only a small fraction of ΔS_{tot}, with the absolute cumulative ΔS_θ ranging from approximately 2 to 12% of the total absolute cumulative ΔS_{tot} across the three study basins. Due to the lack of sufficiently accurate soil moisture observations, this component cannot be directly validated. Each soil moisture sensor has a small sphere of influence (~1 dm^3), and this can hardly be used for validating larger areas, although many microwave scientists do so. However, its simulated seasonal behavior aligns with expected hydrological responses across different land-cover types, showing lower storage in bare soil and higher storage capacity in forested areas. Given its limited contribution to ΔS_{tot}, uncertainties in ΔS_θ are unlikely to substantially affect the ΔS_{gw} estimates.

ΔS_{gw} is calculated in SWEO as the residual term:

$$\Delta S_{gw} = \Delta S_{tot} - \Delta S_{snow} - \Delta S_{sw} - \Delta S_\theta \quad (7)$$

Because ΔS_{gw} depends on the accuracy of the other storage components, its reliability is supported by the combined validation evidence. The strong agreement between SWEO and GRACE for ΔS_{tot}, the close correspondence of ΔS_{snow} and ΔS_{sw} with respectively SNOTEL and USGS observations, and the limited influence of ΔS_θ indicate that the residual ΔS_{gw} is also robust.

Downloaded from iwaponline.com/jwcc/article-pdf/17/9/2513/1637356/jwc2026026.pdf
by Delft University of Technology user

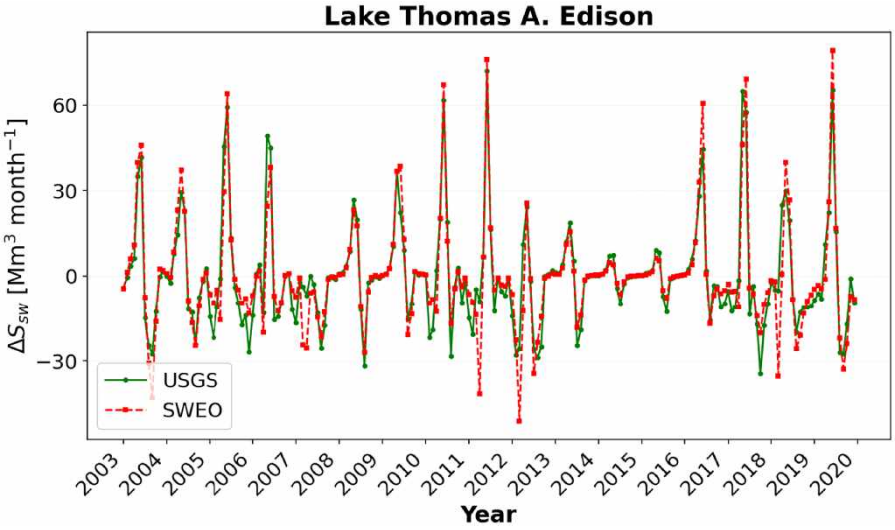


Figure 8 | Temporal comparison of surface water storage changes derived from SWEO and USGS observations (USGS 2025) for Lake Thomas A. Edison (6.7 km^2) in the Upper San Joaquin River Basin.

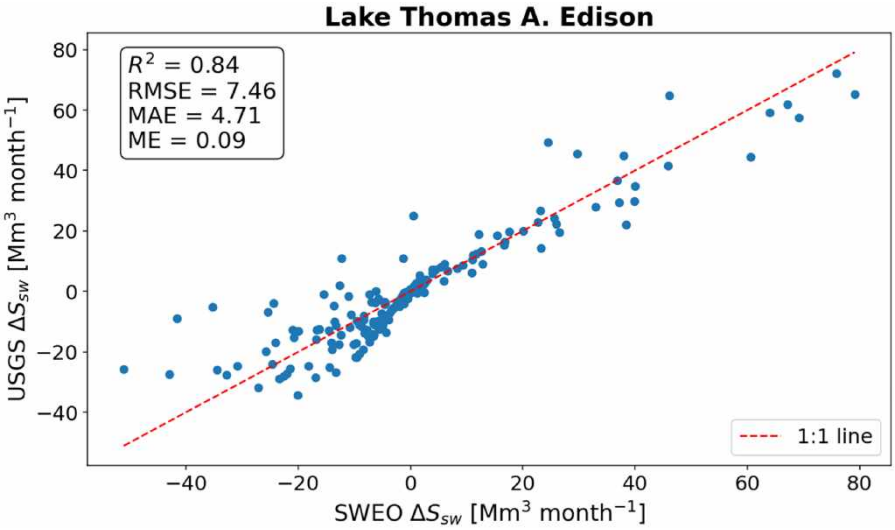


Figure 9 | Correlation analysis between surface water storage changes derived from SWEO and USGS observations (USGS 2025) for Lake Thomas A. Edison (6.7 km^2) in the Upper San Joaquin River Basin.

To support the assessment of groundwater storage ΔS_{gw}, dynamic groundwater heads in SWEO approximated by ΔS_{gw} and specific yield are compared with 201 USGS groundwater head observations in the North Platte River Basin and 13 observations in the San Joaquin River Basin. Figures 12 and 13 present time series comparisons. Across all groundwater observations, an overall R^2 of 0.90 is obtained, as illustrated in Figure 14. The temporal variability of groundwater storage changes in SWEO is thus realistic for the locations inspected. Overall, the spatial agreement between SWEO-derived groundwater heads and observations is good, as indicated by the frequency distribution of ME per observation shown in Figure 14. However, relatively large ME values occur at certain locations, particularly in mountainous regions. These discrepancies are plausibly attributed to the presence of perched groundwater tables, which are not explicitly represented in the current SWEO modeling framework. Accurately simulating such hydrogeological conditions would require a more advanced groundwater model combined with detailed spatial information on soil properties.

Downloaded from iwaponline.com/jwcc/article-pdf/17/9/2513/1637356/jwc2026026.pdf
by Delft University of Technology user

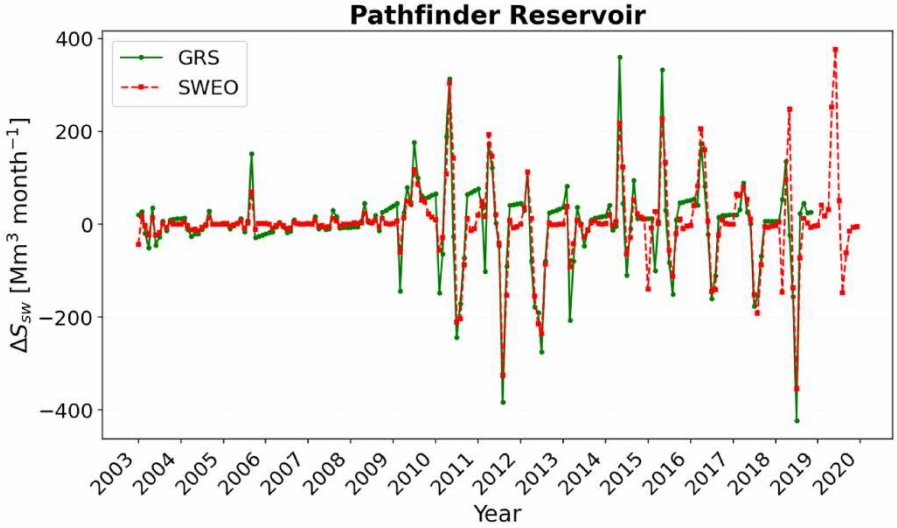


Figure 10 | Temporal comparison of surface water storage changes derived from SWEO and GRS estimates (Li 2023) for Pathfinder Reservoir (75.1 km^2) in the Upper North Platte River Basin.

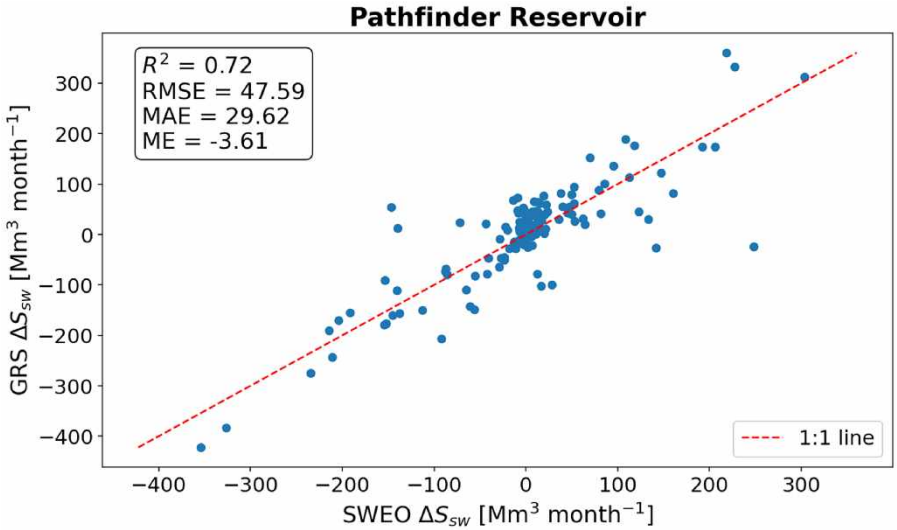


Figure 11 | Correlation analysis between surface water storage changes derived from SWEO and GRS estimates (Li 2023) for Pathfinder Reservoir (75.1 km^2) in the Upper North Platte River Basin.

5.3. Step (iii): validation of total storage change of the drainage area with measured river discharge

The pixel-based routed discharge is shown in Figure 15 for the Aconcagua Basin. This SWEO-derived discharge was validated against 20 independent gauging stations from the three study areas that were not used for model calibration. The comparison showing the R^2, RMSE, MAE, and ME of the individual stations is shown in Table 5. Across 20 stations in the three basins, the average R^2 is 0.73, ranging from 0.34 to 0.92. Figures 16 and 17 present the monthly time series of two discharge stations, one in the Aconcagua basin and one in the North Platte River Basin. High-flow periods test the accuracy of partitioning precipitation into runoff, ET, and aquifer recharge, while low-flow periods reflect the accuracy of groundwater baseflow and surface water withdrawals. The good agreement in both high and low flow regimes indicates that the drainage area monthly bulk storage changes and fluxes are consistently represented within the SWEO water balance.

Downloaded from iwaponline.com/jwcc/article-pdf/17/9/2513/1637356/jwc2026026.pdf
by Delft University of Technology user

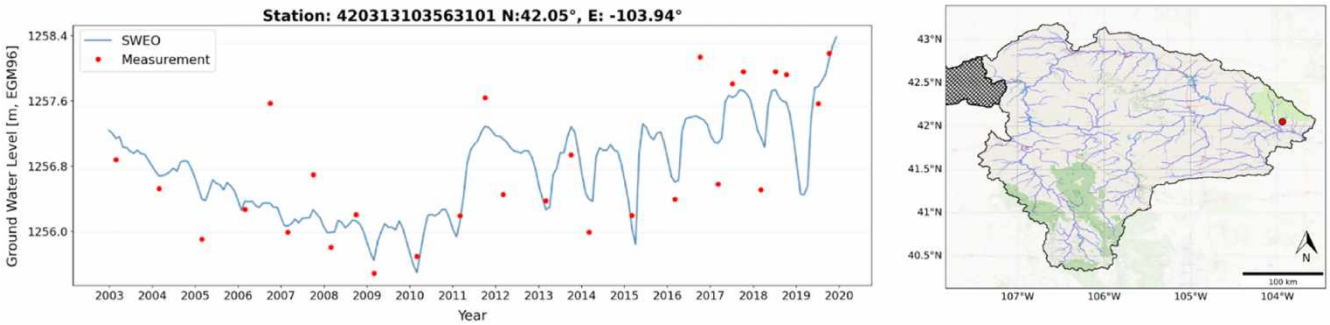


Figure 12 | Temporal comparison of groundwater levels derived from SWEO and USGS station: 420313103563101 in the Upper North Platte River Basin.

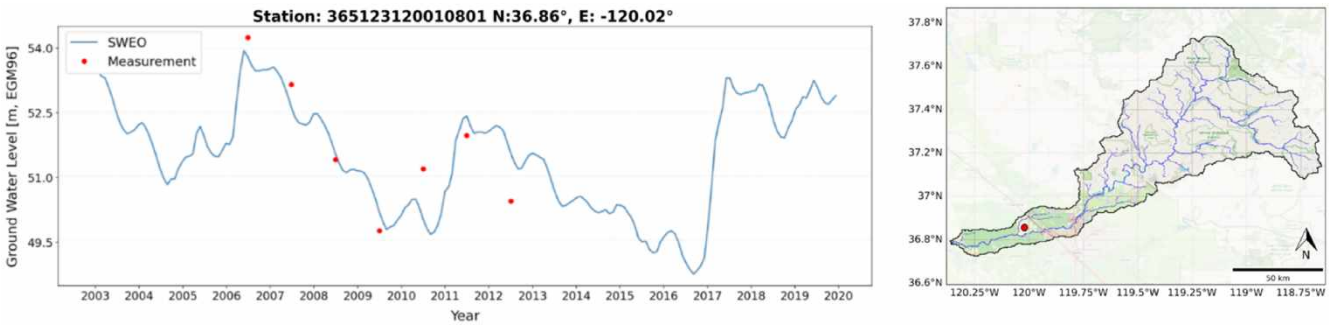


Figure 13 | Temporal comparison of groundwater levels derived from SWEO and USGS station: 365123120010801 in the Upper San Joaquin River Basin.

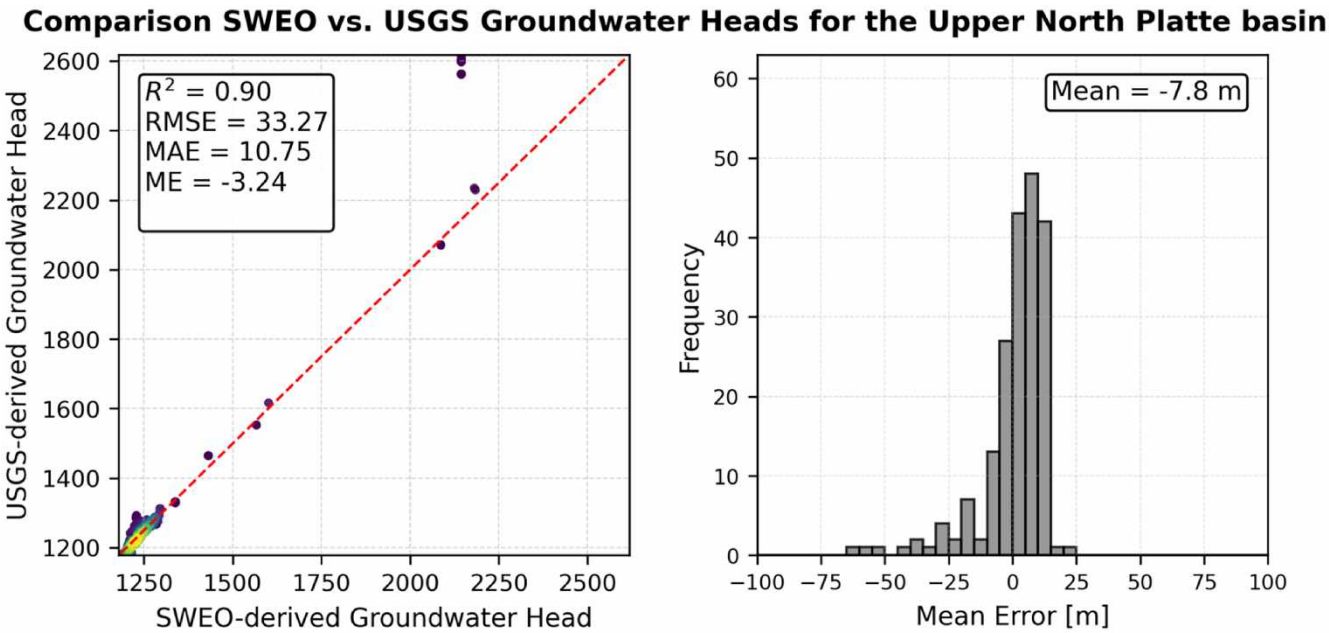


Figure 14 | Validation of groundwater heads in the Upper North Platte River Basin: (a) comparison of SWEO-derived heads with USGS observations, and (b) frequency distribution of mean errors of all USGS observation stations.

Downloaded from iwaponline.com/jwcc/article-pdf/17/9/2513/1637356/jwc2026026.pdf
by Delft University of Technology user

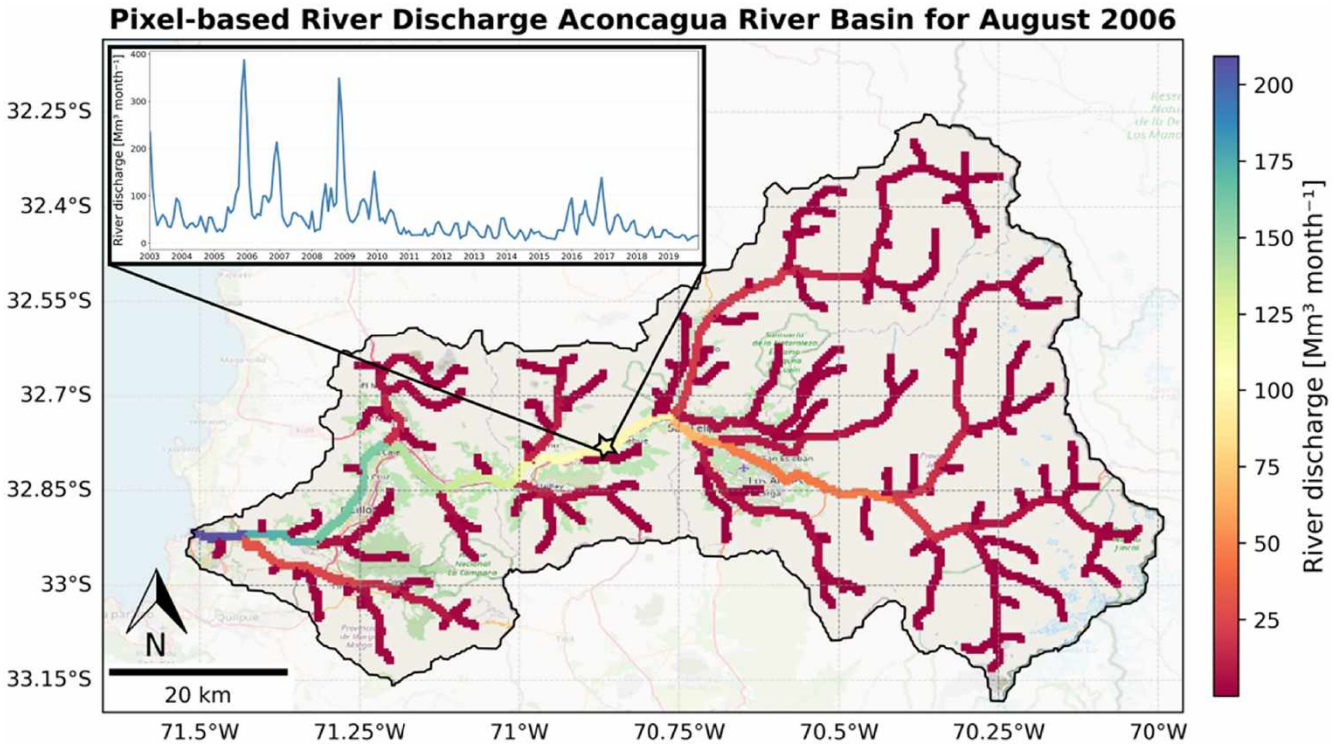


Figure 15 | SWEO pixel-based estimate of discharge over the Aconcagua Basin. Discharge is computed from the upstream pixel-based water surplus combined with the drainage direction map. Each pixel contains the full discharge time series; the map shows values for August 2006 in Mm^3 $month^{-1}$.

These results demonstrate that monthly fluxes and states of the overall water balance are sufficiently accurate for the drainage areas upstream of each discharge station, providing a consistent total water balance. This robust foundation supports the subsequent computation and validation of groundwater withdrawals in the following section.

5.4. Step (iv): validation of groundwater withdrawal

The comparison of annual groundwater withdrawal volumes is shown in Figure 18, which indicates strong agreement between SWEO-derived and USGS-reported values, with an R^2 of 0.91 and a MAE of 13.79 Mm^3 $year^{-1}$. Because this comparison is based on total withdrawal volumes and does not account for differences in withdrawal intensity related to the size of agricultural areas, the total volumes were also normalized by the corresponding irrigated area. The resulting area-averaged groundwater withdrawals yield similarly strong agreement, with an R^2 of 0.90 and a MAE of 36.15 mm $year^{-1}$. This indicates that the strong correlation in total volumes is not solely driven by the size of the irrigated area within the counties but also reflects a consistent representation of groundwater withdrawal intensity.

The results demonstrate that, at the regional scale of administrative counties, yearly groundwater withdrawals for the USA basins are well represented by SWEO. The USGS value of total withdrawal for the San Joaquin Basin was 232 Mm^3 $year^{-1}$ and for SWEO 230 Mm^3 $year^{-1}$, a deviation of 1%. For the entire domain of the Upper North Platte River, the values were 287 and 306 Mm^3 $year^{-1}$ for USGS and SWEO, respectively (7% deviation).

In addition to total groundwater withdrawal volumes, the relative irrigation contribution of groundwater (Q_{gw}/Q_{tot}) was evaluated. In the Aconcagua Basin, SWEO estimates a long-term mean Q_{gw}/Q_{tot} of 37% across irrigated agricultural areas, with a clear downstream increase from approximately 32% upstream of the village Chagres to 45% in the lower basin see Figure 19. This spatial pattern indicates a progressively greater reliance on groundwater for irrigation in downstream areas, where surface water availability is limited. The modeled gradient is consistent with data from the Chilean General Water Directorate (DGA), which show a higher density of groundwater extraction rights for agricultural use in the lower basin. The agreement between these independent data sources suggests that irrigation in the

Downloaded from iwaponline.com/jwcc/article-pdf/17/9/2513/1637356/jwc2026026.pdf
by Delft University of Technology user

Table 5 | Statistical comparison of river discharge derived from SWEO with USGS or DGA observations (DGA 2025; USGS 2025), including the coefficient of determination (R^2), root mean square error (RMSE; $Mm^3\ month^{-1}$), mean absolute error (MAE; $Mm^3\ month^{-1}$), and mean error (ME; $Mm^3\ month^{-1}$)

Basin	Station	Coordinate	Basin area (km^2)	Source	R^2	RMSE	MAE	ME
Aconcagua	5403002	S: 32.91°, E: −70.30°	888	DGA	0.78	16.73	12.29	11.68
Aconcagua	5406001	S: 32.86°, E: −70.41°	828	DGA	0.82	27.73	22.80	22.71
Aconcagua	5410005	S: 32.76°, E: −70.74°	2,968	DGA	0.90	21.31	17.12	14.11
Aconcagua	5411001	S: 32.92°, E: −70.54°	184	DGA	0.92	0.61	0.45	−0.38
Upper San Joaquin	11224000	N: 37.63°, E: −119.09°	115	USGS	0.50	13.60	7.50	−6.11
Upper San Joaquin	11230200	N: 37.31°, E: −118.95°	19	USGS	0.62	1.46	0.74	0.23
Upper San Joaquin	11230500	N: 37.34°, E: −118.97°	136	USGS	0.79	10.48	5.51	−1.01
Upper San Joaquin	11230530	N: 37.34°, E: −118.98°	137	USGS	0.78	10.61	5.33	2.12
Upper San Joaquin	11238600	N: 37.21°, E: −119.33°	3,085	USGS	0.91	86.63	52.15	33.45
Upper San Joaquin	11242000	N: 37.14°, E: −119.45°	3,344	USGS	0.90	79.78	48.97	27.91
Upper San Joaquin	11242400	N: 37.40°, E: −119.57°	48	USGS	0.70	1.59	1.04	−0.61
Upper San Joaquin	11244000	N: 37.29°, E: −119.53°	127	USGS	0.34	5.71	3.42	0.27
Upper San Joaquin	11250110	N: 37.00°, E: −119.71°	4,226	USGS	0.89	9.28	5.01	−1.72
Upper North Platte River	06620000	N: 40.94°, E: −106.35°	3,709	USGS	0.70	38.40	27.28	14.48
Upper North Platte River	06622700	N: 41.37°, E: −106.52°	95	USGS	0.61	3.88	2.65	−0.40
Upper North Platte River	06622900	N: 41.34°, E: −106.52°	91	USGS	0.78	6.22	3.89	−3.83
Upper North Platte River	06627800	N: 41.44°, E: −106.97°	280	USGS	0.61	3.88	2.65	−0.40
Upper North Platte River	06660000	N: 41.33°, E: −105.60°	2,764	USGS	0.72	12.03	7.88	−3.39
Upper North Platte River	06661000	N: 41.29°, E: −106.04°	405	USGS	0.67	15.80	9.91	−9.86
Upper North Platte River	06661585	N: 41.55°, E: −105.69°	4,314	USGS	0.62	21.18	13.09	−0.80
			Total Average		0.73	19.34	12.48	4.92

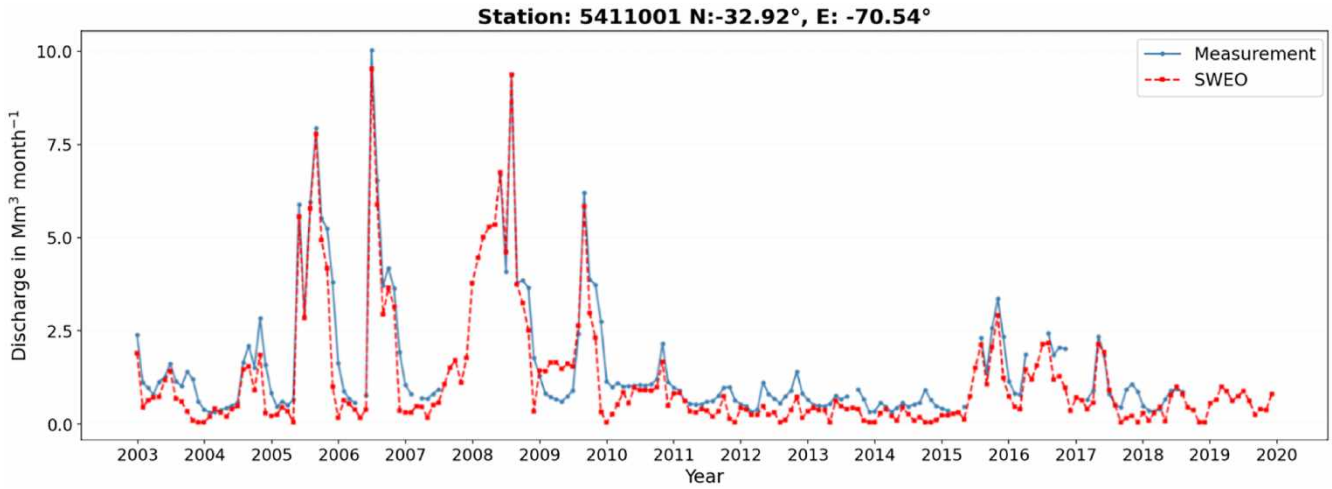


Figure 16 | Comparison of SWEO simulations with DGA observations (DGA 2025) of river discharge at Station 5411001 in the Aconcagua River Basin from 2003 to 2019.

downstream Aconcagua Basin increasingly depends on groundwater abstraction due to less reliable surface water supplies.

The SWEO time-series analysis for 2003–2019 identifies hotspots with pronounced increases in groundwater withdrawals for the Aconcagua basin. These increases are concentrated along the foothills of the Andes and correspond to newly

Downloaded from iwaponline.com/jwcc/article-pdf/17/9/2513/1637356/jwc2026026.pdf
by Delft University of Technology user

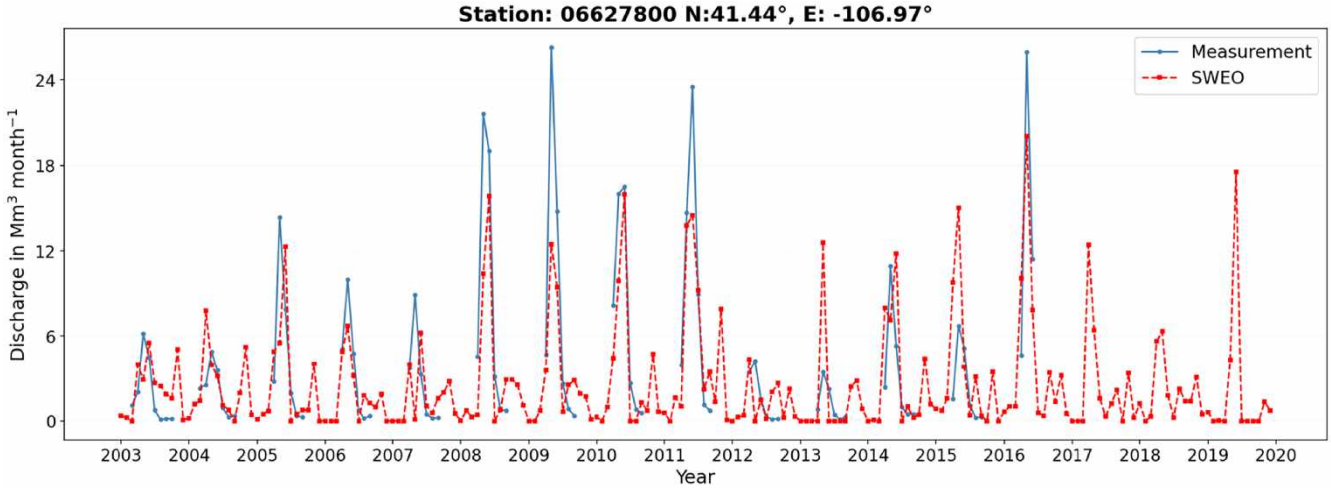


Figure 17 | Comparison of SWEO simulations with USGS observations (USGS 2025) of river discharge at Station 06627800 in the Upper North Platte River Basin from 2003 to 2019.

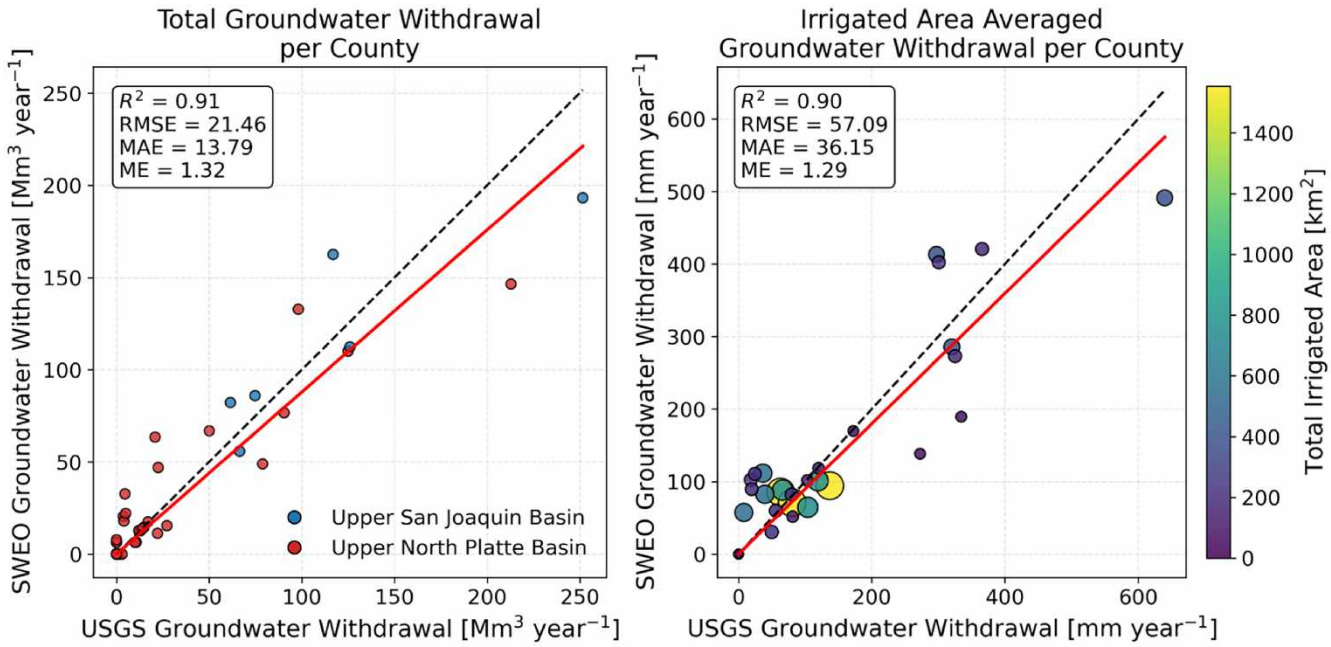


Figure 18 | Comparison of (left) yearly total groundwater withdrawals per county (Mm^3 $year^{-1}$) from SWEO with USGS reports (Kenny *et al.* 2009; Maupin *et al.* 2014; Dieter *et al.* 2018), and (right) average yearly total groundwater withdrawals per county over irrigated areas (mm $year^{-1}$).

established avocado plantations (Figure 20). These plantations occur in both upstream and downstream parts of the basin and are associated with increased groundwater use. Previous studies have already identified a correlation between the expansion of avocado cultivation and the depletion of groundwater resources in the region (Aliaga-Alvarado *et al.* 2023; Durán-Llacer *et al.* 2025). These findings indicate that avocado plantations are highly dependent on groundwater for irrigation, a dependency that is also captured by the SWEO simulations.

In the Upper North Platte Basin, groundwater dependence is comparatively lower, with annual groundwater contributions ranging from 13 to 22% of total irrigation withdrawals. In the surroundings of Scottsbluff, agricultural fields are predominantly irrigated with surface water, consistent with county-level statistics indicating that 76.8–98.6% of irrigation water was supplied by surface sources between 1985 and 2015 (Dieter *et al.* 2018; Wells *et al.* 2020). Figure 21 also

Downloaded from iwaponline.com/jwcc/article-pdf/17/9/2513/1637356/jwc2026026.pdf
by Delft University of Technology user

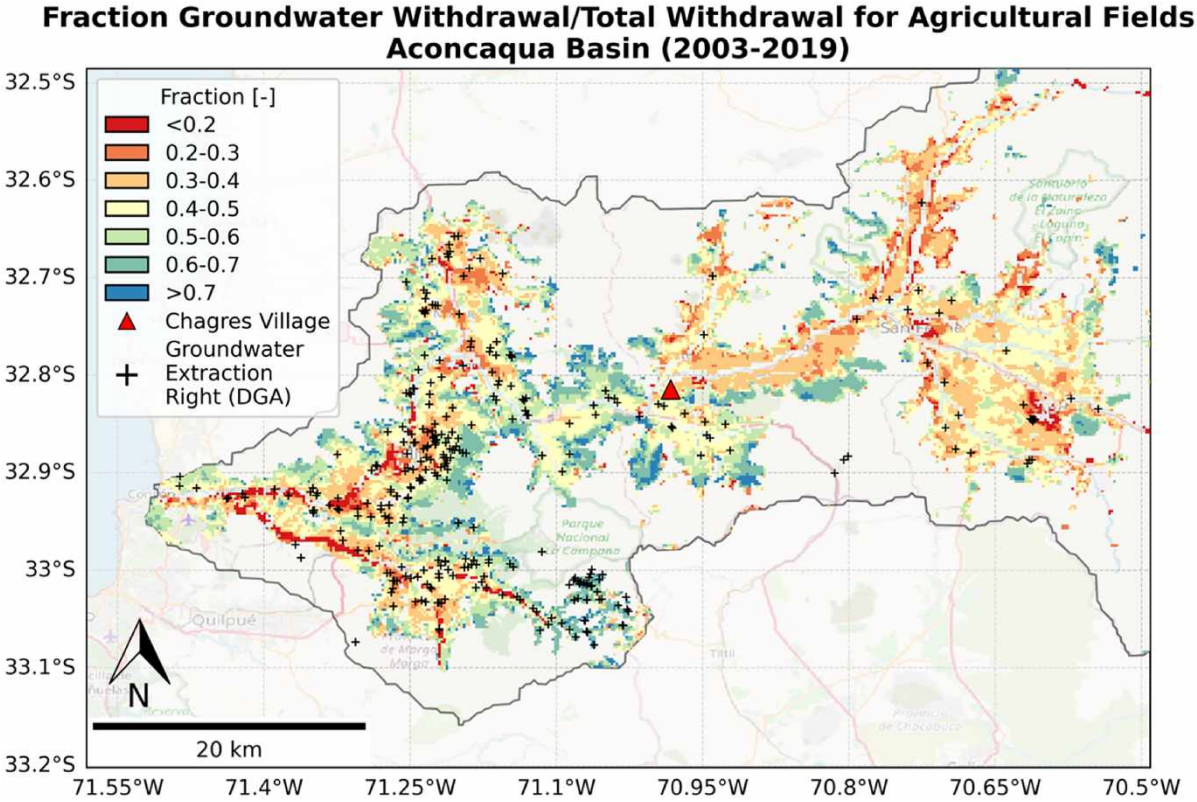


Figure 19 | Ratios of groundwater to total water withdrawal (Q_{gw}/Q_{tot}) for agricultural fields in Aconcagua over 2003–2019. Areas with higher Q_{gw}/Q_{tot} ratios correspond to regions with a higher density of DGA groundwater extraction rights.

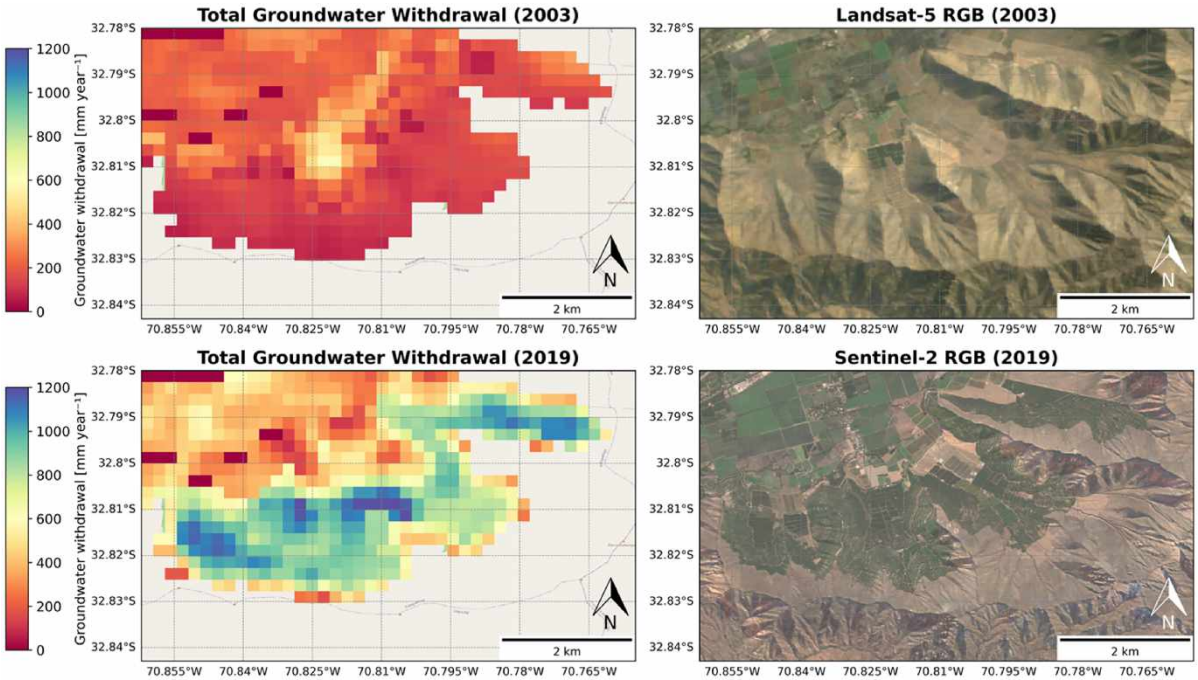


Figure 20 | Comparison of SWEO groundwater withdrawals in the Aconcagua River Basin for 2003 (top row) and 2019 (bottom row), alongside Landsat-5/Sentinel-2 imagery from the corresponding years. Hotspots of increased withdrawals along the foothills correspond to newly established avocado plantations, illustrating SWEO's predicted high dependence on groundwater for irrigation.

Downloaded from iwaponline.com/jwcc/article-pdf/17/9/2513/1637356/jwc2026026.pdf
by Delft University of Technology user

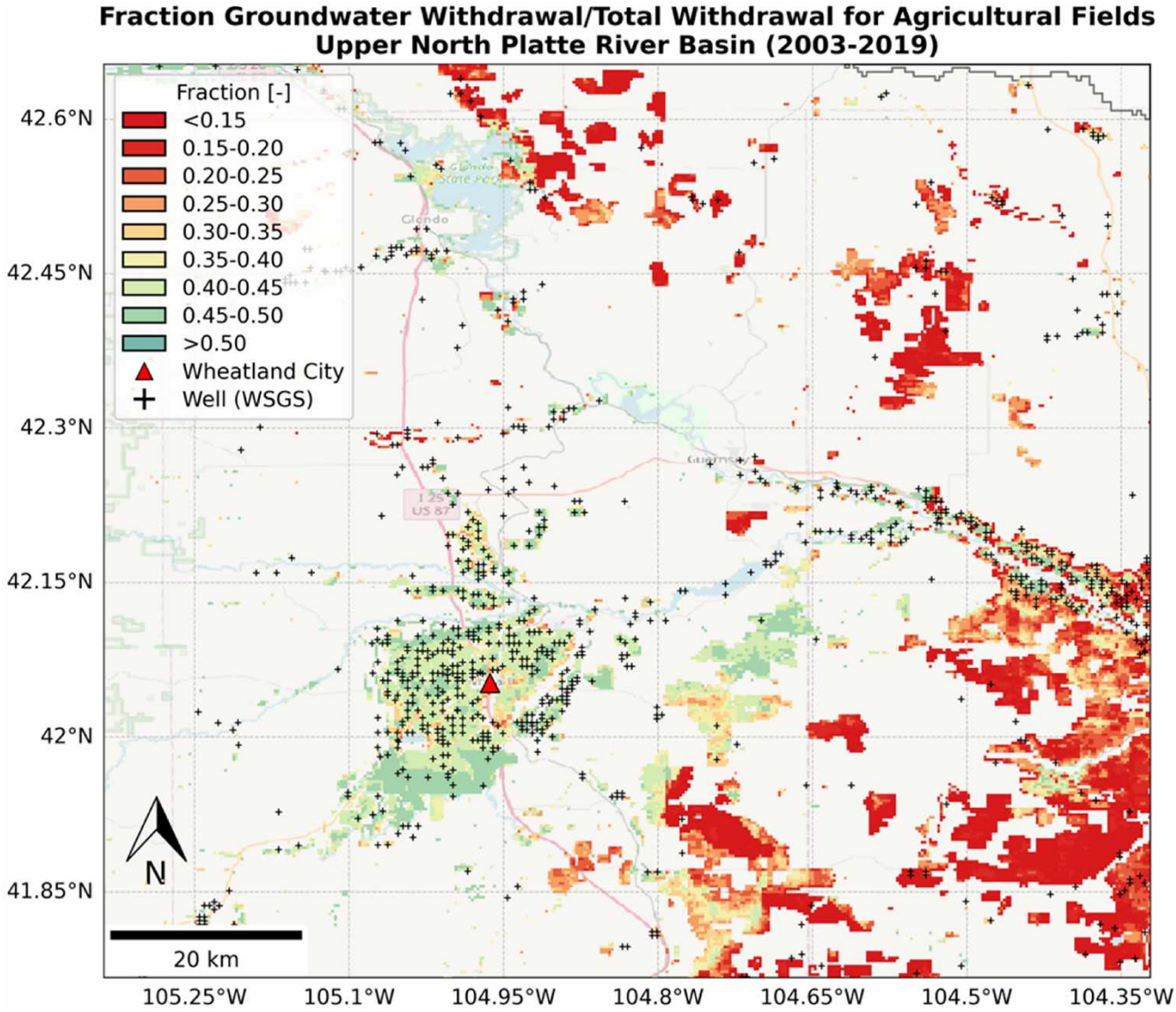


Figure 21 | Ratios of groundwater to total water withdrawal (Q_{gw}/Q_{tot}) for agricultural fields in Upper North Platte River Basin over 2003–2019. Areas with higher Q_{gw}/Q_{tot} ratios correspond to regions with a higher density of wells (WSGS 2025).

shows the locations of agricultural wells obtained from the Wyoming State Geological Survey (WSGS 2025). Notably, the Wheatland irrigation area exhibits a higher reliance on groundwater, with long-term average Q_{gw}/Q_{tot} ratios of approximately 30%. This pattern closely aligns with the spatial distribution of wells, which shows a higher density of agricultural groundwater abstractions in this region. More generally, across the basin, areas with higher well densities correspond to higher modeled fractions of groundwater contribution in the SWEO results.

In the Upper San Joaquin Basin, SWEO simulations indicate substantial groundwater dependence, particularly downstream of Millerton Reservoir. The long-term mean Q_{gw}/Q_{tot} ratio is estimated at 44%, which is consistent with previous studies reporting that approximately 40–48% of total irrigation demand in California's Central Valley is met through groundwater withdrawals (Faunt *et al.* 2016; DWR 2020; Neely *et al.* 2021).

6. LIMITATIONS OF THE METHODOLOGY

Except for precipitation (P), all model parameters are calibrated and bias corrected from mass conservation at particular space and time scales. For this reason, only the uncertainty of P will propagate through the spatially distributed water

Downloaded from iwaponline.com/jwcc/article-pdf/17/9/2513/1637356/jwc2026026.pdf
by Delft University of Technology user

balance for every pixel. In the North Platte River Basin, for example, satellite-based P products tend to underestimate snowfall in mountainous areas, introducing additional uncertainty in groundwater recharge and withdrawal estimates. Hence, P should be calibrated using local gauge measurements prior to start running SWEO. The use of supplementary observations in addition to rain gauges, such as SNOTEL snow measurements, could further improve precipitation corrections in snow-dominated basins. A different solution is to apply cross-validation approaches with other spatial datasets on ET and storage changes to assess the consistency of P data before executing SWEO (Mourad *et al.* 2026). P can only be modified as a pre-processing component.

The methodology further assumes that long-term trends in TWS are minor in magnitude and can be derived adequately from GRACE satellite observations for basin-scale storage variations. However, notable differences exist among GRACE data products, and it is hard to favor a single data set, partially because the spatial resolution of GRACE observations is substantially larger than the spatial resolution of the SWEO grid, which intricate comparisons. Because the long-term changes in TWS generally represent a relatively small component of the total water balance compared with P and ET, uncertainties in GRACE-derived storage trends are believed to have a limited impact on annual river basin scale balances. Nevertheless, the selection of GRACE data sets needs more attention. It has, however, no impact on the SWEO parameterization that can deal with different spatial input data sets.

In this study, ET-bias corrected data were not validated against independent field measurements of ET fluxes. Future work could evaluate different ET products available for SWEO using eddy covariance flux tower observations, scintillometers or surface renewal methods. Regional ET datasets, such as those provided by the University of Nebraska (GloDET), USGS (SSEBop), FAO (WaPOR), and OpenET, could be considered. There are also several scripts available in Google Earth Engine to run own surface energy balance models. Like for storage changes, the selection of the ET data layer will not impact the parameterization process, but may have an impact on local water balances.

Annual averages of reported total groundwater withdrawals per county from USGS were used to compare SWEO outputs. Using yearly bulk data reduces temporal variability and can smooth out short-term fluctuations, potentially resulting in lumping of variables and affecting correlation metrics such as R^2 and MAE. Nonetheless, annual data provide a robust assessment of long-term trends and overall water balance at the basin scale. Where possible, SWEO outputs were also examined at monthly scales to ensure consistency with shorter-term dynamics. The validation of local groundwater withdrawals on individual fields could not be completed in this study, but is recommended to undertake local validations in future studies.

Despite these limitations, the SWEO framework provides a transparent methodology for assessing regional groundwater balances that is consistent with river flow, river-aquifer interactions and percolation water from land surfaces. Although the validation was conducted across three contrasting river basins, these basins cannot represent the full diversity of hydroclimatic conditions, geological settings, and water management practices worldwide. Additional applications in other regions would further strengthen the global applicability of the SWEO framework. A new testing of SWEO in India is foreseen.

7. CONCLUSIONS

Three distinct river basins were used to validate a 250 m gridded water balance integrating atmospheric, soil, river, reservoir, and groundwater components based on open-access data. Across all basins, SWEO demonstrates strong capability to capture the overall water balance through an internal calibration approach that leverages the strengths and compensates for the limitations of diverse, primarily remote sensing datasets. Monthly ΔS_{tot} derived from SWEO shows good agreement with GRACE observations (R^2 = 0.62–0.73), confirming that both seasonal variability and interannual storage dynamics are well reproduced. The accuracy of both ΔS_{tot} and individual storage components confirms the robustness of the water balance, with ΔS_{snow} showing strong correspondence with SNOTEL observations (average R^2 = 0.84; MAE = 35.3 mm month^{-1}) and ΔS_{sw} across reservoirs showing reasonable agreement with observed reservoir storage dynamics (average R^2 = 0.81; MAE = 9.59 Mm^3 month^{-1} for reservoirs with USGS observations), further supported by strong agreement between observed and SWEO-simulated river discharge across 20 gauging stations (average R^2 = 0.73; MAE = 12.48 Mm^3 month^{-1}), indicating that surface and groundwater interactions are effectively represented.

SWEO provides reliable estimates of ΔS_{gw}, forming a firm basis for calibrating recharge to baseflow, and Q_{gw} to 214 groundwater head observations (R^2 = 0.90; MAE = 10.75 m). Simulated Q_{gw} shows good spatial and temporal agreement with reported datasets on a yearly basis, literature values, and the locations of irrigation wells, while capturing expected interannual variability across dry and wet years. Comparison with USGS county-level groundwater withdrawal statistics further shows strong agreement (R^2 = 0.91; MAE = 13.79 Mm^3 year^{-1}), highlighting SWEO's ability to produce spatially

Downloaded from iwaponline.com/jwcc/article-pdf/17/9/2513/1637356/jwc2026026.pdf
by Delft University of Technology user

distributed estimates, useful for both groundwater-dependent ecosystems and groundwater withdrawals for irrigation, a combination rarely covered simultaneously by other approaches. Hence, SWEO outputs with a grid of 250 m are compared against physical measurements (e.g., water tables, water storage, or ET fluxes) that are point-based rather than areal. So it is very impressive to see the high R^2 values, despite these scale mismatches.

The validation results illustrate that SWEO can be used to provide rapid assessments of monthly and annual water balances of large river basins with complex topography and heterogeneous terrain. Processing of river basins in the cloud can be done within a few days. This offers an attractive alternative to conventional numerical surface-groundwater models, particularly in data-scarce basins that require a long period to set them up and calibrate them. Because SWEO relies primarily on globally available remote sensing datasets and does not require detailed hydrogeological information to run, it is highly suitable for application across diverse regions worldwide. The preliminary validation also confirms that key hydrological processes, such as groundwater abstraction patterns, can be effectively inferred from satellite observations. Continued validation and refinement will further enhance the framework, especially as the accuracy and availability of Earth observation datasets improve.

The governance of groundwater is complex due to its invisible and elusive nature. Overall, SWEO complements conventional in situ monitoring networks and provides extra spatially distributed groundwater-related information that otherwise is not available. By providing reliable insights into groundwater recharge, withdrawals, and water storage dynamics, SWEO contributes to more informed and resilient groundwater governance under diverse climatic and anthropogenic pressures. Its outputs support the development of more effective water allocation policies and drought mitigation strategies.

FUNDING

This study did not receive support from any external funding sources.

DATA AVAILABILITY STATEMENT

Data cannot be made publicly available; readers should contact the corresponding author for details.

CONFLICT OF INTEREST

The authors declare there is no conflict.

REFERENCES

Aliaga-Alvarado, M., Gómez-Escalonilla, V. & Martínez-Santos, P. (2023) Identification of non-conventional groundwater resources by means of machine learning in the Aconcagua basin, Chile, *Journal of Hydrology: Regional Studies*, **49**, 101502.

Alvarez-Garreton, C., Boisier, J. P., Garreaud, R., González, J., Rondanelli, R., Gayó, E. & Zambrano-Bigiarini, M. (2024) HESS opinions: the unsustainable use of groundwater conceals a 'Day zero', *Hydrology and Earth System Sciences*, **28** (7), 1605–1616.

Amanambu, A. C., Obarein, O. A., Mossa, J., Li, L., Ayeni, S. S., Balogun, O., Oyebamiji, A. & Ochege, F. U. (2020) Groundwater system and climate change: present status and future considerations, *Journal of Hydrology*, **589**, 125163.

Bastiaanssen, W. G. M. & Hessels, T. M. (2022) *Water Accounts of Selected Chilean River Basins (2003–2019)*. Delft: Delft University of Technology, Partners for Water Programme, Ministry of Foreign Affairs, p. 49.

Bastiaanssen, W. G. M., Cheema, M. J. M., Immerzeel, W. W., Miltenburg, I. & Pelgrum, H. (2012) The surface energy balance and actual evapotranspiration of the transboundary Indus Basin estimated from satellite measurements and the ETLook model, *Water Resources Research*, **48**, W11512. doi:10.1029/2011WR0101482.

California Department of Water Resources (2020) *California's Groundwater: Update 2020 (Bulletin 118)*. Sacramento, CA, USA: California Natural Resources Agency. https://water.ca.gov/Programs/Groundwater-Management/Bulletin-118.

Dieter, C. A., Maupin, M. A., Caldwell, R. R., Harris, M. A., Ivahnenko, T. I., Lovelace, J. K., Barber, N. L. & Linsey, K. S. (2018) *Estimated use of Water in the United States in 2015 (No. 1441)*. Reston, VA, USA: US Geological Survey.

Dinku, T., Hailemariam, K., Maidment, R., Tarnavsky, E. & Connor, S. (2014) Combined use of satellite estimates and rain gauge observations to generate high-quality historical rainfall time series over Ethiopia, *International Journal of Climatology*, **34** (7), 2489–2504.

Dirección General de Aguas (DGA) (2025) Registro de caudales diarios. Available at: https://dga.mop.gob.cl/estadisticas-estaciones-dga/ (Accessed 20 June 2025).

Durán-Llacer, I., Salazar, A. A., Mondaca, P., Rodríguez-López, L., Martínez-Retureta, R., Zambrano, F., Llanos, F. & Frappart, F. (2025) Influence of avocado plantations as driver of land use and land cover change in Chile's Aconcagua Basin, *Land*, **14** (4), 750.

FAO (2020) *WaPOR Database Methodology: Version 2 Release, April 2020*. Rome. https://doi.org/10.4060/ca9894en.

Downloaded from iwaponline.com/jwcc/article-pdf/17/9/2513/1637356/jwc2026026.pdf
by Delft University of Technology user

Faunt, C. C., Sneed, M., Traum, J. & Brandt, J. T. (2016) Water availability and land subsidence in the Central Valley, California, USA, *Hydrogeology Journal*, **24** (3), 675–684.

Funk, C., Peterson, P., Landsfeld, M., Pedreros, D., Verdin, J., Shukla, S., Husak, G., Rowland, J., Harrison, L., Hoell, A. & Michaelsen, J. (2015) The climate hazards infrared precipitation with stations – a new environmental record for monitoring extremes, *Scientific Data*, **2** (1), 150066.

Hengl, T., Mendes de Jesus, J., Heuvelink, G. B., Ruiperez Gonzalez, M., Kilibarda, M., Blagotić, A., Shangguan, W., Wright, M. N., Geng, X., Bauer-Marschallinger, B. & Guevara, M. A. (2017) Soilgrids250m: global gridded soil information based on machine learning, *PLoS one*, **12** (2), e0169748.

Hessels, T. M., Bastiaanssen, W. G. M., Stigter, T. Y., Davids, J. C., Schoups, G. & Perry, C. J. (2026) On the determination of pixel-based groundwater withdrawals using SWEO water accounting procedures. Part 1: methodology, *Journal of Water and Climate Change*.

Hessels, T., Davids, J. C. & Bastiaanssen, W. (2022) Scalable Water Balances from Earth Observations (SWEO): results from 50 years of remote sensing in hydrology, *Water International*, **47** (6), 866–886.

Hessels, T. M. (2015) *Comparison and validation of several open access remotely sensed rainfall products for the Nile Basin*. Delft: Delft University of Technology.

Karimi, P. & Bastiaanssen, W. G. (2015) Spatial evapotranspiration, rainfall and land use data in water accounting–Part 1: review of the accuracy of the remote sensing data, *Hydrology and Earth System Sciences*, **19** (1), 507–532.

Kenny, J. F., Barber, N. L., Hutson, S. S., Linsey, K. S., Lovelace, J. K. & Maupin, M. A. (2009) Estimated use of water in the United States in 2005, *S. Geological Survey Circular*, **1344**, 52.

Li, Y. (2023) 'Global Reservoir Storage (GRS) dataset'. Zenodo. doi:10.5281/zenodo.7855477.

López-Bermeo, C., Montoya, R. D., Caro-Lopera, F. J. & Díaz-García, J. A. (2022) Validation of the accuracy of the CHIRPS precipitation dataset at representing climate variability in a tropical mountainous region of South America, *Physics and Chemistry of the Earth, Parts A/B/C*, **127**, 103184.

MapBiomas (2024) MapBiomas Chile, Version 1.0 2024. https://chile.mapbiomas.org.

Maupin, M. A., Kenny, J. F., Hutson, S. S., Lovelace, J. K., Barber, N. L. & Linsey, K. S. (2014) Estimated use of water in the United States in 2010: U.S, *Geological Survey Circular*, **1405**, 56. https://dx.doi.org/10.3133/cir1405.

Melton, F., Amidi-Abraham, G., Friedrichs, M., Purdy, A., Volk, J., Carrara, W., Yang, Y., Harding, J., Allen, R., Anderson, M. & Tuxin-Bettman, K. (2025). 'OpenET: supporting Sustainable Water Management with Earth Observations and Open Science', *World Environmental and Water Resources Congress 2025*, pp. 567–574.

Mourad, R., Schoups, G., Rajendran, V. & Bastiaanssen, W. (2026) Joint calibration of multi-scale hydrological data sets using probabilistic water balance data fusion: methodology and application to the irrigated Hindon River Basin, India, *Hydrology and Earth System Sciences*, **30** (3), 525–551.

Murböck, M., Abrykosov, P., Dahle, C., Hauk, M., Pail, R. & Flechtner, F. (2023) In-orbit performance of the GRACE accelerometers and microwave ranging instrument, *Remote Sensing*, **15**, 563.

Neely, W. R., Borsa, A. A., Burney, J. A., Levy, M. C., Silverii, F. & Sneed, M. (2021) Characterization of groundwater recharge and flow in California's San Joaquin Valley from InSAR-observed surface deformation, *Water Resources Research*, **57** (4), e2020WR028451.

Pekel, J. F., Cottam, A., Gorelick, N. & Belward, A. S. (2016) High-resolution mapping of global surface water and its long-term changes, *Nature*, **540** (7633), 418–422.

Ren, Z., Che, T., Xu, F., Zhang, Y., Tan, J., Wang, J. & Wang, W. (2025) Validation of remotely sensed evapotranspiration products using optical–microwave scintillometer flux measurements over the heterogeneous surfaces, *IEEE Journal of Selected Topics in Applied Earth Observations and Remote Sensing*, **18**, 5687–5703.

Rivera-Vidal, R., Arumí, J. L., Melo, O., Delgado, V., Parra, V., Stehr, A. & Daniele, L. (2025) Managed aquifer recharge implementation challenges: lessons from Chile's Water-Scarce Regions, *Groundwater for Sustainable Development*, **31**, 101502.

Rusli, S. R., Bense, V. F., Mustafa, S. M. & Weerts, A. H. (2024) The impact of future changes in climate variables and groundwater abstraction on basin-scale groundwater availability, *Hydrology and Earth System Sciences*, **28** (22), 5107–5131.

Śliwińska, J., Nastula, J., Dobslaw, H. & Dill, R. (2020b) Evaluating gravimetric polar motion excitation estimates from the RL06 GRACE monthly-mean gravity field models, *Remote Sensing*, **12** (6), 930.

Śliwińska, J., Wińska, M. & Nastula, J. (2020a) Preliminary estimation and validation of polar motion excitation from different types of the grace and grace follow-on missions data, *Remote Sensing*, **12** (21), 3490.

Sophocleous, M. (2002) Interactions between groundwater and surface water: the state of the science, *Hydrogeology Journal*, **10** (1), 52–67.

Sriwongsitanon, N., Suwawong, T., Thianpopirug, S., Williams, J., Jia, L. & Bastiaanssen, W. (2020) Validation of seven global remotely sensed ET products across Thailand using water balance measurements and land use classifications, *Journal of Hydrology: Regional Studies*, **30**, 100709.

Sutanudjaja, E. H., Van Beek, R., Wanders, N., Wada, Y., Bosmans, J. H., Drost, N., Van Der Ent, R. J., De Graaf, I. E., Hoch, J. M., De Jong, K. & Karssenberg, D. (2018) PCR-GLOBWB 2: a 5 arcmin global hydrological and water resources model, *Geoscientific Model Development*, **11** (6), 2429–2453.

Tapley, B. D., Bettadpur, S., Ries, J. C., Thompson, P. F. & Watkins, M. M. (2004) GRACE measurements of mass variability in the Earth system, *Science*, **305** (5683), 503–505.

Downloaded from iwaponline.com/jwcc/article-pdf/17/9/2513/1637356/jwc2026026.pdf
by Delft University of Technology user

U.S. Department of Agriculture, Natural Resources Conservation Service (2025) Snow Telemetry (SNOTEL) data [Data set]. https://www.nrcs.usda.gov.

U.S. Geological Survey (2020) National Land Cover Database (NLCD) 2020 [Data set]. U.S. Department of the Interior. https://www.usgs.gov/centers/eros/science/national-land-cover-database.

U.S. Geological Survey (2025) USGS National Water Information System (NWIS) [Data set]. https://waterdata.usgs.gov.

Van Ham, D., Hoekstra, A. Y., Wada, Y., Bouraoui, F., de Roo, A., Mekonnen, M. M., Van De Bund, W. J., Batelaan, O., Pavelic, P., Bastiaanssen, W. G. & Kummu, M. (2018) Physical water scarcity metrics for monitoring progress towards SDG target 6.4: an evaluation of indicator 6.4. 2 'Level of water stress', *Science of the Total Environment*, **613**, 218–232.

Vereecken, H., Schnepf, A., Hopmans, J. W., Javaux, M., Or, D., Roose, T., Vanderborght, J., Young, M. H., Amelung, W., Aitkenhead, M. & Allison, S. D. (2016) Modeling soil processes: review, key challenges, and new perspectives, *Vadose Zone Journal*, **15** (5), vzj2015–09.

Wada, Y., Wisser, D. & Bierkens, M. F. (2014) Global modeling of withdrawal, allocation and consumptive use of surface water and groundwater resources, *Earth System Dynamics*, **5** (1), 15–40.

Warmedinger, L., Huber, M., Anand, M., Lehner, B., Walper, C., Gorzawski, L., Thieme, M., Wessel, B. & Roth, A. (2023) 'The new hydrographic hydrosheds database derived from the tandem-X DEM', *IGARSS 2023–2023 IEEE International Geoscience and Remote Sensing Symposium*. IEEE, pp. 1485–1488

Wells, M. J., Gilmore, T. E., Nelson, N., Mittelstet, A. & Böhlke, J. K. (2020) Determination of vadose and saturated-zone nitrate lag times using long-2 term groundwater monitoring data and statistical machine learning, *Hydrology & Earth System Sciences Discussions*, **25**, 811–829.

Western States Groundwater Site (WSGS) Database (2025) Well locations and associated metadata. https://waterplan.state.wy.us/plan/platte/2013/gis/Wells_WSEO_PtRB.html.

Wiese, D. N., Yuan, D.-N., Boening, C., Landerer, F. W. & Watkins, M. M. (2019) JPL GRACE and GRACE-FO Mascon Ocean, Ice, and Hydrology Equivalent Water Height. Ver. RL06Mv02. PO.DAAC, CA, USA. https://doi.org/10.5067/TEMSC-3MJ62 (Accessed 2 March 2025)

Yang, D., Yang, Y. & Xia, J. (2021) Hydrological cycle and water resources in a changing world: a review, *Geography and Sustainability*, **2** (2), 115–122.

First received 15 January 2026; accepted in revised form 3 July 2026. Available online 6 August 2026

Downloaded from iwaponline.com/jwcc/article-pdf/17/9/2513/1637356/jwc2026026.pdf
by Delft University of Technology user